

A Review of Bayesian Uncertainty Quantification in Deep Probabilistic Image Segmentation

M.M.A. Valiuddin, R.J.G. van Sloun*, C.G.A. Viviers*, P.H.N. De With, F. van der Sommen

Abstract—Advancements in image segmentation play an integral role within the broad scope of Deep Learning-based Computer Vision. Furthermore, their widespread applicability in critical real-world tasks has resulted in challenges related to the reliability of such algorithms. Hence, uncertainty quantification has been extensively studied within this context, enabling the expression of model ignorance (*epistemic* uncertainty) or data ambiguity (*aleatoric* uncertainty) to prevent uninformed decision-making. Due to the rapid adoption of Convolutional Neural Network (CNN)-based segmentation models in high-stake applications, a substantial body of research has been published on this very topic, causing its swift expansion into a distinct field. This work provides a comprehensive overview of probabilistic segmentation, by discussing fundamental concepts of uncertainty quantification, governing advancements in the field as well as the application to various tasks. Moreover, literature on both types of uncertainties trace back to four key applications: (1) to quantify statistical inconsistencies in the annotation process due to ambiguous images, (2) correlating prediction error with uncertainty, (3) expanding the model hypothesis space for better generalization, and (4) Active Learning. An extensive discussion follows that includes an overview of utilized datasets for each of the applications and evaluation of the available methods. We also highlight challenges related to architectures, uncertainty quantification methods, standardization and benchmarking, and finally end with recommendations for future work such as methods based on single forward passes and models that appropriately leverage volumetric data.

Index Terms—image segmentation, uncertainty quantification, probabilistic modeling, epistemic, aleatoric

I. INTRODUCTION

IMAGE segmentation entails pixel-wise classification of data, effectively delineating objects and regions of interest [1]. With the rapid development of Convolution Neural Networks (CNNs), Deep Learning-based image segmentation has seen major advancements and gained significant interest over time [2]–[4], obtaining impressive scores with large-scale segmentation datasets [5]–[7]. Nevertheless, such methodologies rely on extensive assumptions and relaxations on the Bayesian learning paradigm, omitting crucial information on the uncertainty associated with the model predictions. This omission diminishes the reliability and interpretability of such models. For example, a difficult distinction between classes in real-time automotive scenarios can result in disastrous consequences or uncertain lesion malignancy prediction may significantly impact the decision-making of invasive treatments.

* = Equal contribution

All authors are affiliated with the Department of Electrical Engineering, Eindhoven University of Technology, The Netherlands.

Contact primary author: m.m.a.valiuddin@tue.nl

Extensive efforts have been made to align modern neural network optimization with Bayesian Machine Learning [8]–[11], such as learning parameter densities, rather than point estimates, to include a notion of *epistemic* uncertainty. Furthermore, explicitly modeling the output likelihood distribution enables expressing the *aleatoric* uncertainty. Notably, literature mentions that determining the nature of uncertainty is not often straightforward. For example, Hüllermeier *et al.* [12] stated that “by allowing the learner to change the setting, the distinction between these two types of uncertainty will be somewhat blurred”. This sentiment is also shared by Kiureghian and Ditlevsen [13], noting that “in one model an addressed uncertainty may be aleatory, in another model it may be epistemic”. Sharing similar views, we highlight the necessity of careful analyses and possible subjective interpretation regarding the topic.

Fortunately, the merits of uncertainty quantification have been well-recognized in the field of CNN-based segmentation and underscore the importance of a rigorous literature overview. Nonetheless, most surveys take the perspective from the medical domain [14], [15], often for specific modalities [16]–[19]. There is a notable absence of a comprehensive overview in this field, relating theoretical foundation to the multitude of applications. Furthermore, the abundance of available works can be often overwhelming for both emerging and seasoned researchers. This study seeks to fill this gap in literature and contributes to the subject area by providing a curated overview, where various concepts are discussed through standardized notation and clarified by mutual comparison. After reading this work, readers will be able to discern various forms of uncertainty with their pertinent applications to segmentation tasks. Additionally, they will have developed comprehensive understanding of challenges and unexplored avenues in the field.

This review paper is structured as follows. Past work with significant impact in general image segmentation is presented in Section II, where closely related surveys are also referenced. Then, the theoretical framework and notation that governs the remainder of the paper is introduced in Section III. The role of these concepts in image segmentation will be treated in Sections IV and V, which include all architectures and approaches with significant impact on the field. We then consider the applications that use these uncertainty estimates in Section VI. Finally, this overview will be further discussed together with key challenges and future recommendations in Section VII, which is concluded in Section VIII. Figure 1 illustrates a brief overview of the sections.

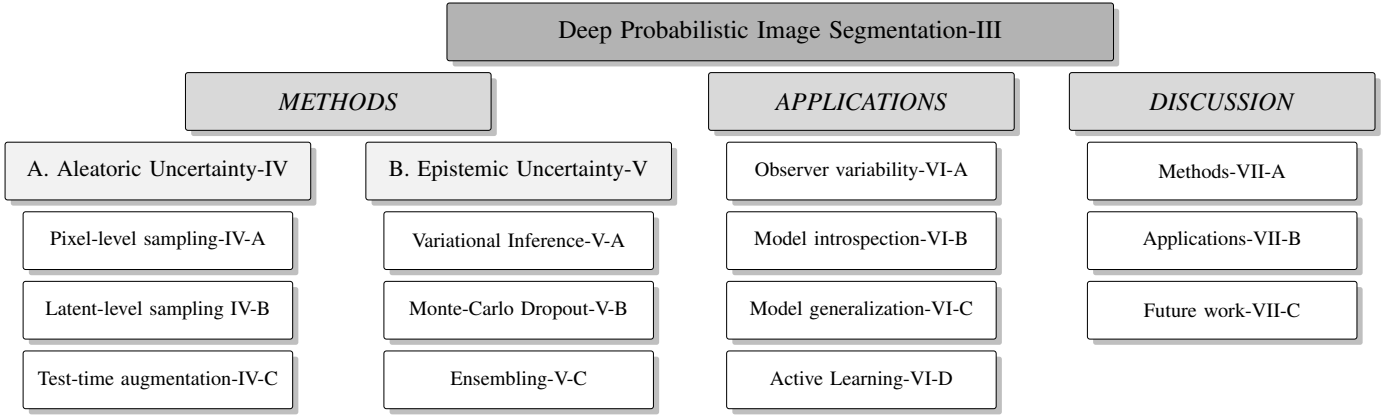


Fig. 1. Overview of the sections. The leaves of the presented hierarchical tree are related to subsections of the article.

II. BACKGROUND

This section highlights a selection of literature crucial to the development of current probabilistic segmentation models. While literature on segmentation itself is vast, this decision has resulted in a limited collection of studies.

As summarized by Minaee *et al.* [20], semantic segmentation has been performed using methods such as thresholding [21], histogram-based bundling, region-growing [22], k-means clustering [23], watershedding [24], to more advanced algorithms such as active contours [25], graph cuts [26], conditional and Markov random fields [27], and sparsity-based methods [28], [29]. After the application of CNNs [30], the domain of image segmentation underwent rapid developments. Notably, the Fully Convolutional Network (FCN) [3] adapted the AlexNet [31], VGG16 [32] and GoogLeNet [33] architectures to enable end-to-end semantic segmentation. Furthermore, other CNN architectures such as DeepLabv3 [34], and the MobileNetv3 [35] have also been commonly used.

As the research progressed, increasing success has been observed with encoder-decoder models [2], [4], [36], [37]. Initially developed for the medical applications, Ronneberger *et al.* [2] introduced the U-Net, which successfully relies on residual connections between the encoding-decoding path, to preserve high-frequency details in the encoded feature maps. To this day, the U-Net is still often utilized as the default backbone model for segmentation architectures, particularly in the medical domain. In fact, reports of recent research indicate that the relatively simple U-Net and nnU-Net [38] still outperform more contemporary and complex models [39], [40].

Semantic segmentation focuses solely on assigning class labels to each pixel and is particularly suitable for amorphous or uncountable subjects of interest. In contrast, instance segmentation not only detects, but also delineates individual objects within the image. This form of segmentation is more applicable when identifying and outlining countable instances of objects. The third category, panoptic segmentation, combines both class and instance-level classification [20].

III. PROBABILISTIC IMAGE SEGMENTATION

This section describes the fundamentals of Bayesian inference and its relationship with conventional models for segmentation. The provided details introduce standard variables and notations as we proceed throughout the manuscript.

A. Bayesian inference

Assuming random-variable pairs $(\mathbf{Y}, \mathbf{X}) \sim P_{\mathbf{Y}, \mathbf{X}}$ that take values in $\mathcal{Y} \in \mathbb{R}^{K \times H \times W}$ and $\mathcal{X} \in \mathbb{R}^{C \times H \times W}$, respectively, then \mathbf{Y} can be considered as the ground-truth of a K -class segmentation task and \mathbf{X} as the query image. The variables H , W and C correspond to the image height, width and channel depth, respectively. Conforming to the principle of maximum entropy, the optimal parameters given the data (i.e. posterior) subject to the chosen intermediate distributions can be inferred through Bayes Theorem as

$$p(\boldsymbol{\theta} | \mathbf{y}, \mathbf{x}) = \frac{p(\mathbf{y} | \mathbf{x}, \boldsymbol{\theta}) p(\boldsymbol{\theta})}{p(\mathbf{y} | \mathbf{x})}, \quad (1)$$

where $p(\boldsymbol{\theta})$ represents the prior belief on the parameter distribution and $p(\mathbf{y} | \mathbf{x})$ the conditional data likelihood (also commonly referred to as the *evidence*). After obtaining a posterior with dataset $\mathcal{D} = \{\mathbf{x}_i, \mathbf{y}_i\}_{i=1}^N$ containing N images, the predictive distribution from a new datapoint \mathbf{x}^* can be denoted as

$$p(\mathbf{Y} | \mathbf{x}^*, \mathcal{D}) = \int \underbrace{p(\mathbf{Y} | \mathbf{x}^*, \boldsymbol{\theta})}_{\text{Data}} \underbrace{p(\boldsymbol{\theta} | \mathcal{D})}_{\text{Model}} d\boldsymbol{\theta}. \quad (2)$$

As evident, both the variability in the empirical data and the inferred parameters of the model influence the predictive distribution. Hence, uncertainties stemming from the conditional likelihood distribution are classified as either *aleatoric*, implying from the statistical diversity in the data, or *epistemic*, which stems from the posterior, i.e. the variance of the model parameters. A straightforward approach to quantify any of these uncertainties is achieved through obtaining the predictive entropy, which can similarly be decomposed as

$$H[\mathbf{Y} | \mathbf{x}^*, \mathcal{D}] = \underbrace{I[\mathbf{y}, \boldsymbol{\theta} | \mathbf{x}^*, \mathcal{D}]}_{\text{epistemic}} + \underbrace{\mathbb{E}_{q(\boldsymbol{\theta} | \mathcal{D})}[H[\mathbf{y} | \mathbf{x}^*, \boldsymbol{\theta}]]}_{\text{aleatoric}}. \quad (3)$$

B. Conventional segmentation

Regardless of the elegantly formulated Bayesian posterior, most practical approaches make use of so-called “deterministic” segmentation networks, which are trained by Maximum Likelihood Estimation (MLE) and is specified as

$$\theta_{\text{MLE}} = \arg \max_{\theta} \log p(\mathbf{y}|\mathbf{x}, \theta), \quad (4)$$

which simplifies the training procedure by taking a point estimate of the posterior. This approximation improves as the training data increases and the model parameter variances approach zero. As such, MLE does not include any prior knowledge on the structure of the parameter distribution. This is typically achieved through Bayesian Maximum A Posteriori (MAP) estimation with

$$\theta_{\text{MAP}} = \arg \max_{\theta} \log p(\mathbf{y}|\mathbf{x}, \theta) + \log p(\theta). \quad (5)$$

For example, assuming Gaussian or Laplacian priors can be a consequence of regularizing the L_2 norm (also known as *ridge regression* or *weight decay*) or L_1 norm of θ , respectively [41], [42]. Additionally, the output of such models can be interpreted as a probability distribution. For instance, consider spatial image dimensions D and a CNN model $f_{\theta} : \mathbb{R}^{C \times D} \rightarrow \mathbb{R}^{K \times D}$ with parameters θ , such that $\mathbf{a} = f_{\theta}(\mathbf{x})$. Then, the output of such model can be regarded as parameters of a Probability Mass Function (PMF) through

$$p(\mathbf{Y} = k | \mathbf{x}^*, \theta) = \frac{e^{\mathbf{a}_k}}{\sum_k e^{\mathbf{a}_k}}, \quad (6)$$

with channel-wise indexing over the denominator, which is commonly known as the SoftMax activation (Figure 2). This approach is probabilistic modeling in the technical sense, although it is not referred to as such in common nomenclature. In fact, the approximated distribution can represent and localize uncertain regions.

However, the implicit pixel-independence assumption

$$p(\mathbf{Y}|\mathbf{X}) = \prod_i^{K \times D} p(Y_i|\mathbf{X}), \quad (7)$$

omits information on structural variation in the segmentation masks. At the very core, this limitation (See Figure 3) has driven research on probabilistic segmentation, enabling the sampling of spatially coherent segmentation masks. This challenge can be addressed either from the aleatoric or epistemic perspective. Both approaches have relevant specific use cases, and distinct merits and drawbacks, as will become clear in the upcoming sections.

IV. ALEATORIC UNCERTAINTY

Aleatoric uncertainty quantification reconsiders the non-deterministic relationship between $\mathbf{x} \in \mathcal{X}$ and $\mathbf{y} \in \mathcal{Y}$, which implies that

$$p(\mathbf{Y}|\mathbf{X}) = \frac{p(\mathbf{Y}, \mathbf{X})}{p(\mathbf{X})} \neq \delta(\mathbf{Y} - F(\mathbf{X})), \quad (8)$$

with Dirac-delta function δ , and mapping $F : \mathcal{X} \rightarrow \mathcal{Y}$. This relationship is characterized by the ambiguity in \mathbf{X} and is

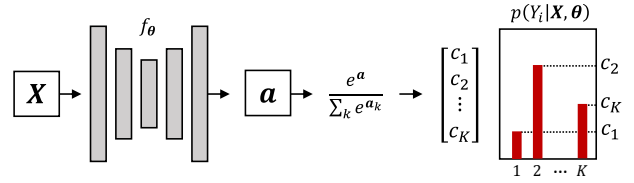


Fig. 2. Aleatoric uncertainty quantification by modeling pixel-level outputs as parameters of a Probability Mass Function.

inherently probabilistic, due to various reasons such as noise in the data (occlusions, sensor noise, insufficient resolution, etc.) or variability within a class (e.g. not all cats have tails). Hence, the observance of substantial aleatoric uncertainty can in some cases be inevitable, but may also signal the need for higher-quality data acquisition or shifting to another modality. The possible input dependency of the uncertainty develops into further categorization of either *heteroscedastic* (dependent) or *homoscedastic* (independent) aleatoric uncertainty.

In most practical scenarios, aleatoric uncertainty quantification methods encompass both types and assume a parameterized likelihood function $p(\mathbf{Y}|\mathbf{X}, \theta)$ as a direct reflection of $p(\mathbf{Y}|\mathbf{X})$. For example, it is possible to model a distribution parameterized by the output of a CNN (Section IV-A). Also, generative models have been used extensively, where the data likelihood is learned through latent variables (Section IV-B). Finally, image augmentation during test-time inference can be also applied to obtain a notion of aleatoric uncertainty (Section IV-C).

A. Pixel-level sampling

A valid approach employs direct pixel-level uncertainty in the annotations. In case the independence assumption holds, it is important to ensure proper calibration of the model, which is discussed in Section IV-A1. In another method, the spatial correlation is explicitly modeled across the pixels of the segmentation mask and results in spatially coherent samples, which will be treated in Section IV-A2.

1) **Independence:** The normalized confidence values that result from SoftMax activation can only be interpreted as probabilities after proper validation, which is referred to as *model calibration*. Ideally, the empirical accuracy of a model should

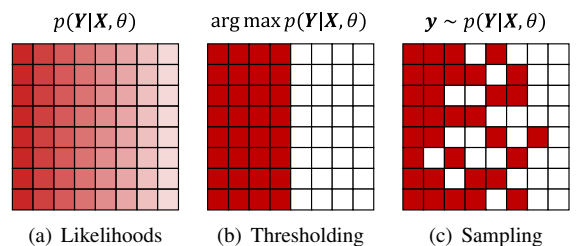


Fig. 3. Illustration of the likelihood function in segmentation models. Color intensities reflect the normalized confidence values that can be interpreted as probabilities. (a) The continuous output results in a horizontal gradient. (b) Maximum likelihood thresholding can be applied. (c) However, the coherence of the segmentation suffers when sampling.

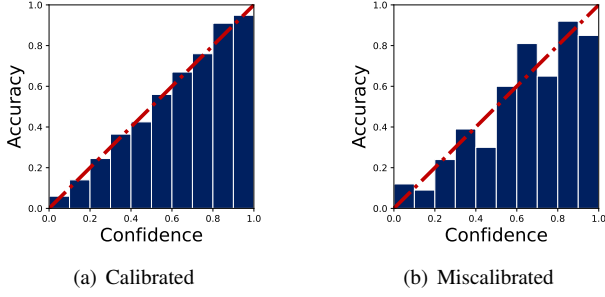


Fig. 4. Visualization of a reliability diagram indicating if the model confidences accurately reflect the empirical probabilities.

be approximately equal to the provided class confidence c_k for class k , i.e. $P(Y = k | c_k) = c_k$. Calibration is typically visualized with a reliability diagram, where miscalibration and under-/over-confidence can be assessed by inspecting the deviation from the graph diagonal (Figure 4). Different methods can be used to measure calibration, but often introduce their own biases. A fairly straightforward metric, the Expected Calibration Error (ECE), determines the normalized distance between accuracy (acc) and confidence (conf) bins as

$$E_{\text{ECE}} = \sum_{b=1}^B \frac{n_b}{N} |\text{acc}(b) - \text{conf}(b)|, \quad (9)$$

with n_b the number of samples in bin b and N being the total sample size across all bins. The ECE is prone to skew representations if some bins are significantly more populated with samples due to over-/under-confidence. Furthermore, the Maximum Calibration Error (MCE) is more appropriate for high-risk applications, where only the worst bin is considered.

Contemporary SoftMax-activated neural networks often portray a significantly incongruous reflection of the true data uncertainty because of negative log-likelihood optimization and techniques such as batch normalization, weight decay and other forms of regularization [9]. Most calibration techniques are post-hoc, i.e. they occur after training and thus require a separate validation set. For example, Temperature Scaling [9] has been applied in a pixel-wise manner for segmentation problems [43]. Nonetheless, some methods, such as Label Smoothing [44], [45] or using the Focal Loss [46] can be directly applied on the training data. Furthermore, overfitting has often been considered to be the cause of overconfidence [47], [48] and erroneous pixels can therefore be penalized through regularizing low-entropy outputs [49].

2) **Spatial correlation**: To explicitly model spatial correlation within pixel space of the likelihood distribution, Mon-

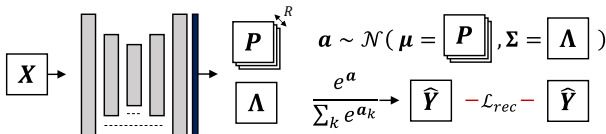


Fig. 5. Depiction of Stochastic Segmentation Networks [50]. Here, the covariance of the likelihood distribution is explicitly modeled through a low-rank approximation.

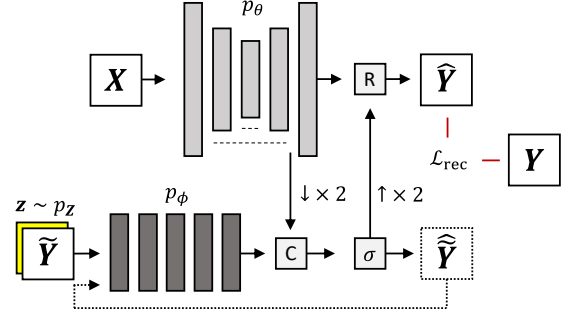


Fig. 6. Illustration of the PixelCNN-based PixelSeg [53]. Parameter ‘C’ indicates the concatenation module, ‘R’ the resampling module and σ the softmax activation. Dotted elements appear during test-time sampling.

teiro *et al.* [50] propose the Stochastic Segmentation Network (SSN), which models the output logits as a multivariate normal distribution, parameterized by the neural networks f_{θ}^{μ} and f_{θ}^{Σ} as

$$p(\mathbf{a}|\mathbf{x}, \theta) = \mathcal{N}(\mathbf{a}; \boldsymbol{\mu} = f_{\theta}^{\mu}(\mathbf{x}), \boldsymbol{\Sigma} = f_{\theta}^{\Sigma}(\mathbf{x})), \quad (10)$$

where the covariance matrix has a low-rank structure

$$\boldsymbol{\Sigma} = \mathbf{P}\mathbf{P}^T + \boldsymbol{\Lambda}. \quad (11)$$

Here, \mathbf{P} has dimensionality $((K \times D) \times R)$, with R being a hyperparameter that controls the parameterization rank and $\boldsymbol{\Lambda}$ a diagonal matrix. This results in a more structured and expressive distribution, while retaining reasonable efficiency. As the SoftMax transform on this low-rank multivariate normal distribution pertains an intractable integral, Monte Carlo sampling is employed. SSNs can be augmented as an additional layer to any existing CNN (see Figure 5).

Another method uses an autoregressive approach to predict pixel Y_i based on the preceding pixels. In this case, we can rephrase Equation (7) to

$$p(\mathbf{Y}|\mathbf{X}) = \prod_i^{K \times D} p(Y_i|Y_1, \dots, Y_{i-1}, \mathbf{X}). \quad (12)$$

A popular method to model such relationship due to its substantial receptive field is known as the PixelCNN [51], [52]. Zhang *et al.* [53] suggest to use this network to predict a down-sampled segmentation mask $\tilde{\mathbf{y}}$ with $p_{\phi}(\tilde{\mathbf{y}}|\mathbf{x})$, and fuse this with a conventional CNN to predict the full-resolution mask with $p_{\theta}(\mathbf{y}|\tilde{\mathbf{y}}, \mathbf{x})$. The two masks are fused through a resampling module, containing a series of specific transformations to improve quality and diversity of the samples. Figure 6 illustrates this concept. Notably, PixelCNNs employ a recursive sampling process, which also enables completion/inpainting of user-given inputs.

B. Latent-level sampling

Directly learning the conditional data distribution is a challenging task. Hence, generative models often employ a simpler latent (unobserved) variable $\mathbf{Z} \sim p_{\mathbf{Z}}$ with $\mathbf{z} \in \mathbb{R}^d$, to instead learn the approximate joint density $p(\mathbf{Y}|\mathbf{Z}, \mathbf{X})$. The marginalized distribution is obtained through integral

$$p_{\theta, \psi}(\mathbf{Y}|\mathbf{X}) = \int p_{\theta}(\mathbf{Y}|\mathbf{z}, \mathbf{X}) p_{\psi}(\mathbf{z}|\mathbf{X}) d\mathbf{z}, \quad (13)$$

with parameters θ, ψ . Conditioning the latent density on the input images is not a necessity, but usually preferred for smooth optimization trajectories [54]. As such, the spatial correlation is not explicitly modeled, rather induced through mapping the latent variables to segmentation masks. Notable generative model architectures relevant to this section are Generative Adversarial Networks (Section IV-B1), Variational Autoencoders (Section IV-B2) and Denoising Diffusion Probabilistic Models (Section IV-B3).

1) **Generative Adversarial Networks (GANs)**: A straightforward approach is to simply learn the marginalization in Equation (13) through sampling from an unconditional prior density

$$p_{\mathbf{z}} = \mathcal{N}(\boldsymbol{\mu} = \mathbf{0}, \boldsymbol{\Sigma} = \mathbf{I}), \quad (14)$$

and mapping this to segmentation \mathbf{Y} through a *generator* $G_\phi : \mathcal{X} \times \mathcal{Z} \rightarrow \mathcal{Y}$. Goodfellow *et al.* [55] show that this approach can be notably enhanced through the incorporation of a discriminative function (the *discriminator*), denoted as $D_\psi : \mathbb{R}^{C \times D} \rightarrow [0, 1]$. In this way, G_ϕ learns to reconstruct realistically looking images through the discriminative capabilities of D_ψ , making sufficient guidance from D_ψ to G_ϕ imperative. We can denote the cost of G_ϕ in the GAN as the negative cost of D_ψ as

$$J_{G_\phi} = -J_{D_\psi} = \mathbb{E}_{p_{\mathcal{D}}}[\log D_\psi(\mathbf{y})] - \mathbb{E}_{p_{\mathcal{Z}}}\mathbb{E}_{p_{\mathcal{D}}}[\log(1 - D_\psi(G_\phi(\mathbf{z}, \mathbf{x})))] \quad (15)$$

While conditional GANs have been used for semantic segmentation earlier [57], Kassapis *et al.* [56] explicitly contextualized the architecture within aleatoric uncertainty quantification, using their proposed Calibrated Adversarial Refinement (CAR) network (see Figure 7). The calibration network, $F_\theta : \mathbb{R}^{C \times D} \rightarrow \mathbb{R}^{K \times D}$, initially provides a SoftMax activated prediction as $F_\theta(\mathbf{x}) = \mathbf{c}$, with (cross-entropy) reconstruction loss

$$\mathcal{L}_{\text{rec}} = -\mathbb{E}_{p_{\mathcal{D}}}[\log p_\theta(\mathbf{c}|\mathbf{x})]. \quad (16)$$

Then, the conditional refinement network G_θ uses \mathbf{c} together with \mathbf{X} and latent samples $\mathbf{z}_i \sim p_{\mathcal{Z}}$ injected at multiple decomposition scales i , to predict various segmentation maps. Furthermore, the refinement network is subject to the adversarial objective

$$\mathcal{L}_{\text{adv}} = -\mathbb{E}_{p_{\mathcal{D}}}\mathbb{E}_{p_{\mathcal{Z}}}[\log D_\psi(G_\phi(F_\theta(\mathbf{x}), \mathbf{z}), \mathbf{x})], \quad (17)$$

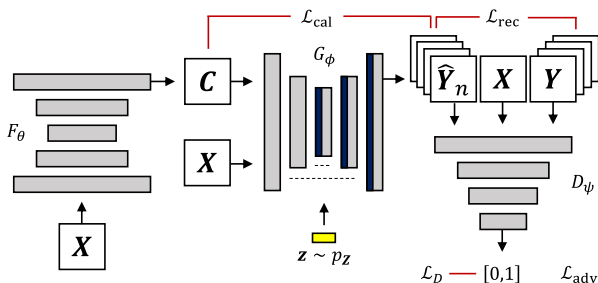


Fig. 7. Diagram of the Calibrated Adversarial Refinement network [56], based on the Generative Adversarial Network with additional loss terms.

which is argued to elicit superior structural qualities compared to relying solely on cross-entropy loss. At the same time, the discriminator opposes the optimization with

$$\mathcal{L}_D = -\mathbb{E}_{p_{\mathcal{Z}}}\mathbb{E}_{p_{\mathcal{D}}}[1 - \log D_\psi(G_\phi(F_\theta(\mathbf{x}), \mathbf{z}), \mathbf{x})] - \mathbb{E}_{p_{\mathcal{D}}}[\log D_\psi(\mathbf{y})]. \quad (18)$$

Finally, the average of the N segmentation maps generated from G_ϕ are compared against the initial prediction of F_θ through the calibration loss, which is the analytical KL-divergence between the two categorical densities, denoted by

$$\mathcal{L}_{\text{cal}} = \mathbb{E}_{p_{\mathcal{D}}} \text{KL}[p_\phi(\mathbf{y}|\mathbf{c}, \mathbf{x}) || p_\theta(\mathbf{c}|\mathbf{x})]. \quad (19)$$

In this way, the generator loss can be defined as

$$\mathcal{L}_G = \mathcal{L}_{\text{adv}} + \lambda \cdot \mathcal{L}_{\text{cal}}, \quad (20)$$

with hyperparameter $\lambda \geq 0$. The purpose of the calibration network is argued to be threefold. Namely, it (1) sets a calibration target for \mathcal{L}_{cal} , (2) provides an alternate representation of \mathbf{X} to G_ϕ , and (3) allows for sample-free aleatoric uncertainty quantification. The refinement network can be seen as modeling the spatial dependency across the pixels, which enables sampling coherent segmentation maps through latent variable \mathbf{Z} .

2) **Variational Autoencoders (VAEs)**: Augmenting a Normalizing Flow (NF) to the posterior density of a VAE is a commonly used tactic to improve its expressiveness [58]. This phenomenon has also been successfully applied to VAE-like models such as the PU-Net [59], [60]. NFs are a class of generative models that utilize k consecutive bijective transformations $f_k : \mathbb{R}^D \rightarrow \mathbb{R}^D$ as $\mathbf{f} = f_K \circ \dots \circ f_k \circ \dots \circ f_1$, to express exact log-likelihoods of arbitrarily complex distributions $\log p(\mathbf{x}|\mathbf{z})$, where symbol \circ indicates functional composition. These are often denoted as $\log p(\mathbf{x})$ for simplicity and can be determined through

$$\log p(\mathbf{x}) = \log p_{\mathcal{Z}}(\mathbf{z}_0) - \sum_{k=1}^K \log \left| \det \frac{df_k(\mathbf{z}_{k-1})}{d\mathbf{z}_{k-1}} \right|, \quad (21)$$

where \mathbf{z}_k and \mathbf{z}_{k-1} are intermediate variables from intermediate densities and $\mathbf{z}_0 = \mathbf{f}^{-1}(\mathbf{x})$. Equation (21) can be substituted in the conditional ELBO objective in Equation (25) to obtain

$$p(\mathbf{Y}|\mathbf{X}) \geq \mathbb{E}_{q_\theta(\mathbf{z}|\mathbf{Y}, \mathbf{X})}[\log p_\phi(\mathbf{Y}|\mathbf{z}, \mathbf{X})] - \text{KL}[q_\theta(\mathbf{z}_0|\mathbf{Y}, \mathbf{X}) || q_\psi(\mathbf{z}|\mathbf{X})] - \mathbb{E}_{q_\theta(\mathbf{z}_0|\mathbf{Y}, \mathbf{X})} \left[\sum_{k=1}^K \log \left| \det \frac{df_k(\mathbf{z}_{k-1})}{d\mathbf{z}_{k-1}} \right| \right], \quad (25)$$

where the objective consists of a reconstruction term, sample-based KL-divergence and a likelihood correction term for the change in probability density induced by the NF.

Bhat *et al.* [61], [62] compare this approach with other parameterizations of the latent space, including a mixture of Gaussians and low-rank approximation of the full covariance matrix. Valiuddin *et al.* [63] show that the latent space can converge to contain non-informative latent dimensions, undermining the capabilities of the latent-variable approach,

generally referred to as mode or posterior collapse [64], [65]. Their proposition considers the alternative formulation of the ELBO, specified as

$$\begin{aligned} \log p(\mathbf{Y}|\mathbf{X}) &\geq \mathbb{E}_{q_\theta(\mathbf{z}|\mathbf{Y},\mathbf{X})} [\log p_\phi(\mathbf{Y}|\mathbf{X},\mathbf{z})] \\ &\quad - \text{KL}[q_\theta(\mathbf{z}|\mathbf{X}) || p_\psi(\mathbf{z}|\mathbf{X})] \\ &\quad - I(\mathbf{Y}, \mathbf{Z}|\mathbf{X}). \end{aligned} \quad (23)$$

The proposed novel objective maximizes the contribution of the (expected) mutual information between latent and output variables. This can be rewritten into the objective

$$\begin{aligned} \mathcal{L} = &-\mathbb{E}_{q_\theta(\mathbf{z}|\mathbf{Y},\mathbf{X})} [\log p_\phi(\mathbf{Y}|\mathbf{X},\mathbf{z})] \\ &+ \alpha \cdot \text{KL}[q_\theta(\mathbf{z}|\mathbf{Y},\mathbf{X}) || p_\psi(\mathbf{z}|\mathbf{X})] \\ &+ \beta \cdot S_\epsilon[q_\theta(\mathbf{z}|\mathbf{X}) || p_\psi(\mathbf{z}|\mathbf{X})], \end{aligned} \quad (24)$$

with S_ϵ being the Sinkhorn divergence [66] and α, β denoting hyperparameters. This adaptation results in a more uniform latent space leading to increased model performance. Also, modeling the ELBO of the joint density has been explored [67]. This formulation results in an additional reconstruction term and forces the latent variables to be more congruent with the data. Furthermore, constraining the latent space to be discrete has resulted in some improvements, where it is hypothesized that this partially addresses the model collapse phenomenon [68].

a) *Density parameterization*: Techniques such as GANs rely on implicit distributions and are void of any notion of data likelihoods. An alternative approach estimates the Bayesian posterior w.r.t. the latent variables, $p(\mathbf{Z}|\mathbf{Y}, \mathbf{X})$, with an approximation $q_\theta(\mathbf{Z}|\mathbf{Y}, \mathbf{X})$, obtained by maximizing the conditional Evidence Lower Bound (ELBO)

$$\begin{aligned} p(\mathbf{Y}|\mathbf{X}) &= \mathbb{E}_{q_\theta(\mathbf{z}|\mathbf{Y},\mathbf{X})} [\log p(\mathbf{Y}|\mathbf{X})] \\ &= \mathbb{E}_{q_\theta(\mathbf{z}|\mathbf{Y},\mathbf{X})} \left[\log \frac{p(\mathbf{z}, \mathbf{Y}|\mathbf{X})}{p(\mathbf{z}|\mathbf{Y}, \mathbf{X})} \right] \\ &\geq \mathbb{E}_{q_\theta(\mathbf{z}|\mathbf{Y},\mathbf{X})} [\log p_\phi(\mathbf{Y}|\mathbf{z}, \mathbf{X})] \\ &\quad - \text{KL}[q_\theta(\mathbf{z}|\mathbf{Y}, \mathbf{X}) || q_\psi(\mathbf{z}|\mathbf{X})]. \end{aligned} \quad (22)$$

This approach of estimating $p(\mathbf{Z}|\mathbf{Y}, \mathbf{X})$ is also known as Variational Inference (VI). The first term in Equation (25) represents the reconstruction cost of the decoder subject to the latent code \mathbf{Z} and input image \mathbf{X} . The second term is the Kullback-Leibler (KL) divergence between the approximate posterior and prior density. As a consequence of the mean-field approximation, all involved densities are modeled by axis-aligned Gaussian densities and amortized through neural networks, parameterized by ϕ, θ and ψ . The predictive distribution after observing dataset \mathcal{D} is then obtained as

$$p(\mathbf{Y}|\mathbf{x}^*) = \int p_\phi(\mathbf{Y}|\mathbf{z}, \mathbf{x}^*) q_\theta(\mathbf{z}|\mathcal{D}) d\mathbf{z}. \quad (26)$$

The implementation of the conditional ELBO in Equation (25) can be achieved through a VAE-like architecture [10]. A few additional design choices specific for uncertainty quantification in segmentation lead to the Probabilistic U-Net (PU-Net) [69]. Firstly, the latent variable \mathbf{Z} is only introduced at the final layers of a U-Net conditioned on \mathbf{X} , where the vector is up-scaled through tiling and then concatenated with the feature

maps of the penultimate layer, which is followed by a sequence of 1×1 convolution for classification. When involving conditional latent variables in this manner, it is expected that most of the semantic feature extraction and delineation are performed in the U-Net, while the provided information by \mathbf{Z} is almost exclusively related to the segmentation variability. Therefore, relatively smaller values of d are feasible than what is commonly used in conventional image generation tasks.

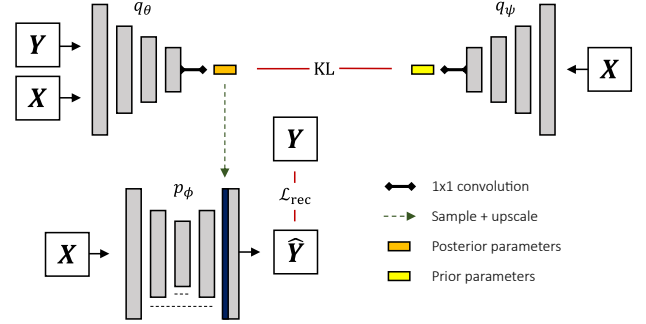


Fig. 8. Depiction of the Probabilistic U-Net [69] based on a conditional Variational Autoencoder [10]. The latent samples are inserted at the final stages of a U-Net through a tiling operation.

Similar to related research on the VAE [58], [65], [70]–[72], much work has been dedicated to improving the PU-Net. For instance, investigation on improving VI with novel parameterization of the amortized densities also provides insights into model behaviour [59]–[62], [67], [68], [73] (Section IV-B2a). Furthermore, extending the architecture to multiple decomposition hierarchies [74], [75] (Section IV-B2b), three-dimensional modalities [76]–[80] (Section IV-B2c), and conditioning on the annotator [81] (Section IV-B2d), also result in substantial performance gains.

b) *Multi-scale approach*: Learning latent features over several hierarchical scales can provide expressive densities and interpretable features across various abstraction levels [82]–[86]. Such models are commonly categorized under hierarchical VAE (HVAE) modeling. Often, an additional Markov assumption of length T is placed on the posterior as

$$q_\theta(\mathbf{Z}_{1:T}|\mathbf{Y}, \mathbf{X}) = q_\theta(\mathbf{Z}_1|\mathbf{Y}, \mathbf{X}) \prod_{t=2}^T q_\theta(\mathbf{Z}_t|\mathbf{Z}_{t-1}). \quad (27)$$

Consequently, the conditional ELBO is denoted as

$$\begin{aligned} p(\mathbf{Y}|\mathbf{X}) &\geq \mathbb{E}_{q_\theta(\mathbf{z}|\mathbf{Y},\mathbf{X})} [\log p_\phi(\mathbf{Y}|\mathbf{z}, \mathbf{X})] \\ &\quad - \sum_{t=2}^T \text{KL}[q_\theta(\mathbf{z}_t|\mathbf{Y}, \mathbf{X}, \mathbf{z}_{1:t-1}) || q_\psi(\mathbf{z}_t|\mathbf{z}_{1:t-1})] \\ &\quad - \text{KL}[q_\theta(\mathbf{z}_1|\mathbf{Y}, \mathbf{X}) || q_\psi(\mathbf{z}_1|\mathbf{X})]. \end{aligned} \quad (28)$$

This objective is implemented in the Hierarchical PU-Net [74] (HPU-Net, depicted in Figure 9). Simply stated, the architecture learns a latent representation at multiple decomposition levels of the U-Net. Furthermore, residual connections in the convolutional layers are necessary to prevent degeneracy of uninformative latent variables with the KL divergence rapidly approaching zero. For similar reasons, the Generalized ELBO

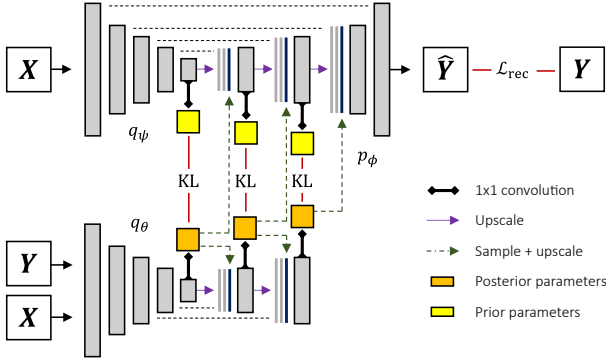


Fig. 9. Hierarchical Probabilistic U-Net [74] based on a hierarchical Variational Autoencoder [10], [82], [84]. Instead of a single latent code, multiple decomposition scales encode the segmentation variability, depending on the depth of the U-Net structure.

with Constrained Optimization (GECO) objective is employed, which extends Equation (28) to

$$\begin{aligned} \mathcal{L}_{\text{GECO}} = & \lambda \cdot (\mathbb{E}_{q_\theta(\mathbf{z}|\mathbf{Y}, \mathbf{X})}[\log p_\phi(\mathbf{Y}|\mathbf{z}, \mathbf{X})] - \kappa) \\ & - \sum_{t=2}^T \text{KL}[q_\theta(\mathbf{z}_t|\mathbf{Y}, \mathbf{X}, \mathbf{z}_{1:t-1}) || q_\psi(\mathbf{z}_t|\mathbf{z}_{1:t-1})] \\ & - \text{KL}[q_\theta(\mathbf{z}_1|\mathbf{Y}, \mathbf{X}) || q_\psi(\mathbf{z}_1|\mathbf{X})]. \end{aligned} \quad (29)$$

Hyperparameter λ is the Lagrange multiplier update through the Exponential Moving Average of the reconstruction, which is constrained to reach target value κ , empirically set beforehand to an appropriate value. Finally, online negative hard mining is used to only backpropagate 2% of the worst performing pixels, which are stochastically picked with the Gumbel-SoftMax trick [87], [88]. A similar architecture known as PHiSeg [75] takes a similar approach to the HPU-Net. However, instead of placing the residual connections in the convolutional layers, PHiSeg uses these between the latent vectors across the decompositions. Furthermore, *deep supervision* at each decomposition scale is used to enforce disentanglement across latent variables.

c) *Extension to 3D*: Early methods for uncertainty quantification in medical imaging primarily utilized 2D slices from three-dimensional (3D) datasets, leading to a potential loss of critical spatial information and subtle nuances often necessary for accurate delineation. This limitation has spurred extensive research into 3D probabilistic segmentation techniques with ELBO-based models, aiming to preserve the integrity of entire 3D structures. Initial works [79], [80] demonstrate that the PU-Net can be adapted by replacing all 2D operations with their 3D variants. Crucially, the fusion of the latent sample with 3D extracted features is achieved through a 3D tiling operation. Viviers *et al.* [78] additionally augment a Normalizing Flow to the posterior density, as described in Section IV-B2a. Further enhancements to the architecture include the implementation of the 3D HPU-Net [77], an updated feature network incorporating the attention mechanisms, a nested decoder, and different reconstruction loss components tailored to specific applications [76].

d) *Conditioning on annotator*: It can be relevant to model the annotators independently in cases with consistent annotator-segmentation pairs in the dataset. This can

be achieved by conditioning the learned densities on the annotator itself [81], [89]. For example, features of a U-Net can be combined with samples from annotator-specific Gaussian-distributed posteriors [89]. Considering the approach from Gao *et al.* [81], generating a segmentation mask is achieved by first sampling an annotator from a categorical prior distribution $\mathcal{C}(\pi_k(\mathbf{x}))$, governed by the image conditional parameters $\pi_k(\mathbf{x})$ for the k -th annotator. Then, samples are taken from its corresponding prior density as $\mathbf{z}_k \sim p_k(\mathbf{z}_k)$ to reconstruct a segmentation through an image-conditional decoder $\mathbf{y} = F(\mathbf{x}, \mathbf{z}_k)$. The parameters $\pi_k(\mathbf{z}_k)$ can also be used to weigh the corresponding predictions to express the uncertainty in the prediction ensemble. Additionally, consistency between the model and ground-truth distribution is enforced through an optimal transport loss between the set of predictions and labels.

3) Denoising Diffusion Probabilistic Models (DDPMs):

Recent developments in generative modeling have resulted in a family of models known as Denoising Diffusion Probabilistic Models [90]–[92]. Such models are especially renowned for their expressive power by being able to encapsulate large and diverse datasets. While several perspectives can be used to introduce the DDPMs, we build upon the earlier discussed HVAE (Section IV-B2b) to maintain cohesiveness with the overall manuscript.

Specifically, we introduce three additional modifications to the HVAE [93]. Firstly, the latent dimensionality is set equal to the spatial data dimensions, i.e. $d=D$. As a consequence, redundant notation of \mathbf{Z} is removed and \mathbf{Y} is instead subscripted with $t \in \{1, \dots, T\}$, indicating the encoding depth, where \mathbf{Y}_0 is the initial segmentation mask. Secondly, the encoding process (or *forward process*) is predefined as a linear Gaussian model such that

$$q(\mathbf{y}_T|\mathbf{y}_0) = p(\mathbf{y}_0) \prod_{t=1}^T q(\mathbf{y}_t|\mathbf{y}_{t-1}), \quad (30)$$

where

$$q(\mathbf{y}_t|\mathbf{y}_{t-1}) = \mathcal{N}(\mathbf{y}_t; \boldsymbol{\mu} = \sqrt{\alpha_t}\mathbf{y}_{t-1}, \boldsymbol{\Sigma} = (1 - \alpha_t) \cdot \mathbf{I}), \quad (31)$$

with noise schedule $\boldsymbol{\alpha} = \{\alpha_t\}_{t=1}^T$. Then, the decoding or *reverse process* can be learned through $p_\phi(\mathbf{y}_{t-1}|\mathbf{y}_t, \mathbf{x})$. The ELBO for this objective is defined as

$$\begin{aligned} p(\mathbf{y}|\mathbf{x}) \geq & \mathbb{E}_{q(\mathbf{y}_1|\mathbf{y}_0)}[\log p_\phi(\mathbf{y}_0|\mathbf{y}_1, \mathbf{x})] \\ & + \sum_{t=2}^T \mathbb{E}_{q(\mathbf{y}_t|\mathbf{Y}_0)}[\text{KL}[q(\mathbf{y}_{t-1}|\mathbf{y}_t) || p_\phi(\mathbf{y}_{t-1}|\mathbf{y}_t, \mathbf{x})]] \\ & + \underbrace{\mathbb{E}_{q(\mathbf{y}_T|\mathbf{y}_0)}\left[\log \frac{p(\mathbf{y}_T)}{q(\mathbf{y}_T|\mathbf{y}_0)}\right]}_{\approx 0}. \end{aligned} \quad (32)$$

As denoted, the regularization term is assumed to be zero, since it is assumed that a sufficient amount of steps T are taken such that $q(\mathbf{y}_T|\mathbf{y}_0)$ is approximately normally distributed. With the reparameterization trick [10], the forward process is governed by random variable $\epsilon \sim \mathcal{N}(0, 1)$. As such, the KL divergence in the second term can be interpreted as predicting \mathbf{Y}_0 , the source noise ϵ or the score $\nabla_{\mathbf{y}_t} \log q(\mathbf{y}_t)$

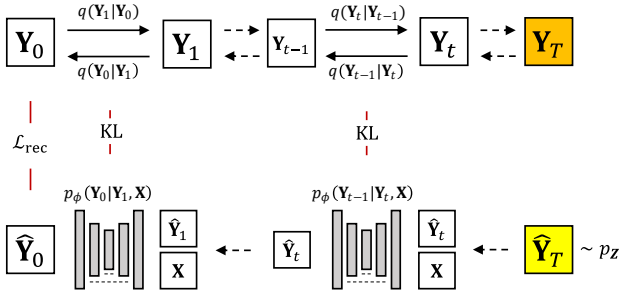


Fig. 10. Illustration of the Diffusion Probabilistic Models [90]. The model learns to remove noise that has been gradually added to the input image.

(gradient of the data log-likelihood) from \mathbf{Y}_t , depending on the parameterization. This is in almost all instances approximated with a U-Net [2].

Also, it has been proposed to model Bernoulli noise instead of Gaussian [94]–[97]. However, most methodologies vary in the conditioning of the reverse process on the input image [98]–[101]. For instance, Wolleb *et al.* [98] concatenate the input image with the noised segmentation mask. Wu *et al.* [99] insert encoded image features to the U-Net bottleneck. Additionally, information on predictions \mathbf{Y}_t at a time step t is provided in the intermediate layers of the conditioning encoder. This is performed by applying the Fast Fourier Transform (FFT) on the U-Net encoding, followed by a learnable attention map and the inverse FFT. The procedure of applying attention on the spectral domain of the U-Net encoding has also been implemented with transformers in follow-up work [100]. Segdiff [101] also encode both current time step and input image, but combine the extracted features by simple summation prior to inferring it through the U-Net.

C. Test-time augmentation

An image \mathbf{X} can be understood as a one-of-many visual representations of the object of interest. For example, systematic noise, translation or rotation result in many realistic variations that approximately retain image semantics. Hence, data augmentation [31] has been used at test time (explaining the name test-time augmentation, or TTA) for image classification, to obtain uncertainty estimates by efficiently exploring the locality of the likelihood function [102]. This technique has been applied to image segmentation as well [103]–[106]. By randomly augmenting input images with invertible transformation $\tilde{\mathbf{x}} = T_\zeta(\mathbf{x})$, with transformation parameters ζ , a prediction is obtained with $\tilde{\mathbf{y}} = f_\theta(\tilde{\mathbf{x}})$ and can then be inverted through $\mathbf{y} = T_\zeta^{-1}(\tilde{\mathbf{y}})$. Repeatedly performing this procedure results in a set of segmentation masks, which serve as an estimate of $p(\mathbf{Y}|\mathbf{X}, \theta)$.

V. EPISTEMIC UNCERTAINTY

The crucial difference between epistemic and aleatoric uncertainty is that the former relates to model ignorance, while the latter reflects statistical ambiguity inherent in the data. Epistemic uncertainty can be further categorized into two distinct types [12]. The first type pertains uncertainty

related to the capacity of the model. For example, underparameterized models or approximate model posteriors, that can become too stringent to appropriately resemble the true posterior. The ambiguity on the best parameters given the limited capacity induces uncertainty in the learning process, which is also known as *model uncertainty*. Nevertheless, given the complexity of contemporary parameter-intensive CNNs, the model uncertainty is often assumed to be negligible. A more significant contribution to the epistemic uncertainty is due to the limited data availability, known as *approximation uncertainty*, and can often be reduced by collecting more data. Both model and approximation uncertainty contribute to the epistemic uncertainty.

Unfortunately, evaluation of the true Bayesian posterior (formulated in Equation (1)) is inhibited by the intractability of the data-likelihood in the denominator. Hence, extensive efforts have been taken to obtain viable approximations, such as using Mean-Field Variational Inference [8], Markov Chain Monte Carlo (MCMC) [107], Monte-Carlo Dropout [108], [109], Model Ensembling [110], Laplace approximations [111], Stochastic Gradient MCMCs [112]–[114], assumed density filtering [115] and expectation propagation [116], [117]. We refer to any neural network that approximates the Bayesian posterior of the model parameters as a Bayesian Neural Network (BNN). The following sections treat applied methodologies to segmentation, which are usually straightforward extensions of conventional regression and classification BNN networks. These techniques are illustrated in Figure 11.

A. Variational Inference

Consider a simpler, tractable density $q(\theta|\eta)$, parameterized by η , to approximate posterior $p(\theta|\mathbf{y}, \mathbf{x})$. Then, we can employ Variational Inference (VI) w.r.t. to the parameters, by minimizing the Kullback-Leibler (KL) divergence between the true and approximated Bayesian posterior as

$$\begin{aligned} \eta^* &= \arg \min_{\theta} \text{KL} [q(\theta|\eta) || p(\theta|\mathbf{y}, \mathbf{x})] \\ &= \arg \min_{\theta} \int q(\theta|\eta) \log \frac{q(\theta|\eta)}{p(\mathbf{Y}|\mathbf{x}, \theta)p(\mathbf{x}, \theta)} d\theta \\ &= \arg \min_{\theta} \text{KL} [q(\theta|\eta) || p(\theta)] - \mathbb{E}_{q(\theta|\eta)} [\log p(\mathbf{y}|\mathbf{x}, \theta)], \end{aligned} \quad (34)$$

where the parameter-independent terms are constant and therefore excluded from notation. A popular choice for the approximated variational posterior is the Gaussian distribution, i.e. a mean μ and covariance σ parameter for each element of the convolutional kernel, usually with zero-mean unitary Gaussian prior densities. However, the priors can be also learned through Empirical Bayes [118]. Furthermore, backpropagation is possible with the *reparameterization trick* [10] and within this context, the procedure is referred to as Bayes by Backprop (BBB) [8]. During testing, a sample-based approach is utilized to approximate the posterior. Using several parameter permutations effectively enriches the hypothesis space due to the model combining effect, and can improve performance [119]–[121].

B. Monte Carlo Dropout

Dropout is a common technique used to regularize neural networks [122] and can mimic sampling from an implicit parameter distribution $q(\tilde{\theta}|\theta, p)$. This implicit distribution is defined as

$$\mathbf{n} \sim \text{Bernoulli}(p), \quad (34a)$$

$$\tilde{\theta} = \theta \odot \mathbf{n}, \quad (34b)$$

with probability p and vector \mathbf{n} operating element-wise on the parameters. Using Dropout can also be interpreted as a first-order equivalent L_2 regularization with additionally transforming the input with the inverse diagonal Fisher information matrix [122]. Using *Monte-Carlo Dropout* (MC Dropout), the random node switching is continued during test time, effectively sampling new sets of parameters. While seemingly arbitrary, it has been shown that MC Dropout can be interpreted as approximate VI in a Deep Gaussian Process [108]. In this manner, such method is able to provide multi-modal estimates of the model uncertainty.

As noted by Gal *et al.* [123], the model output variance is balanced with the weight magnitudes rather than the dropout rate p , which is usually optimized through grid search or simply set to 0.5. Hence, the authors propose to additionally learn p using gradient-based methods, known as Concrete Dropout, such that uncertainty estimates are governed by p . As the name suggests, a continuous approximation to the discrete distribution is used, known as the Concrete distribution [87], [124], to enable path-wise derivatives through p .

C. Model Ensembling

As mentioned earlier, MC dropout effectively optimizes over a set of sparse neural networks. Also, this ensemble can be designed in an explicit manner. To this end, we define the set of functions $\mathbf{f} = \{f_{\theta}^n\}_{n=1}^N$, with N representing the number of models in the ensemble. Then, it is relatively simple to obtain $\Theta = \{\theta_n\}_{n=1}^N$, which can be interpreted as samples from an approximate posterior. Ensembling in only the latter parts of a neural network (typically the decoder) is referred to as M-heads, i.e. the network has multiple outputs. Often, the N obtained parameters are from N separate training sessions. However, it has also been proven effective to ensemble from a single training session, by saving the parameters at multiple stages or training with different weight initializations [125]–[127].

A closely related concept to ensembling is known as Mixture of Experts (MoE), where each model in the ensemble (an ‘expert’) is trained on specific subsets of the data [128]. In such settings, a gating mechanism is usually applied after combining the expert hypotheses. While uncommon, incorporating all predictions can also be regarded as an ensembling technique.

VI. APPLICATIONS

This section explores literature that employs uncertainty-based downstream tasks on segmentation models. These include estimating the segmentation mask distribution subject to

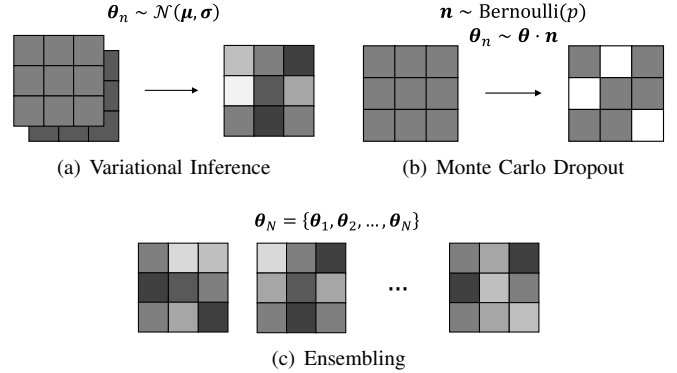


Fig. 11. Three types of techniques are visualized to sample parameters of the convolutional kernels, (a) an approximation of the parameter density can be made, (b) taking samples can be mimicked with dropout during test time, or, (c) an ensemble of N different configurations can be explicitly modeled.

observer variability (Section VI-A), model introspection (i.e. ability to self-assess, Section VI-B), improved generalization (Section VI-C), and reduced labeling costs using Active Learning (Section VI-D).

A. Observer variability

After observing sufficient data, the variability in the predictive distribution is often considered to be negligible and is therefore omitted. Nevertheless, this assumption becomes excessively strong in ambiguous modalities, where its consequence is often apparent with multiple varying, yet plausible annotations for a single image. Additionally, such annotations can also vary due to differences in expertise and experience of annotators. The phenomenon of inconsistent labels across annotators is known as the *inter-observer* variability, while variations from a single annotator are referred to as the *intra-observer* variability (see Figure 12).

To contextualize this phenomenon within the framework of uncertainty quantification, annotators can be regarded as models themselves. For example, consider K separate annotators modeled through parameters ϕ_k with $k = 1, 2, \dots, K$. For a simple segmentation task, it can be expected that $\text{Var}[p(\phi_k)] \rightarrow 0$. In other words, each annotator is consistent in his delineation and the *intra-observer* variability is low. For cases with consensus across experts, i.e. yielding negligible *inter-observer* variability, the marginal approaches to $\text{Var}[p(\phi)] \rightarrow 0$. Asserting these two assumptions, it is valid to simply consider a point estimate of the posterior. Yet, this is rarely the case in many real-life applications and, as such, explicitly modeling the involved distributions becomes necessary.

For evaluation, a commonly used metric minimizes the squared distance between arbitrary mean embeddings of the ground truth and predicted annotations using the kernel trick [129]. This metric is known as Maximum Mean Discrepancy (MMD) or the Generalized Energy Dis-

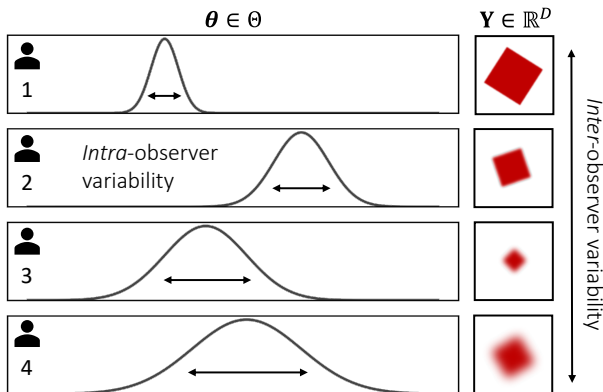


Fig. 12. Visualization of the intra-observer variability in parameter space (left) and the inter-observer variability in data space (right).

tance (GED) [130], denoted as

$$\begin{aligned} \text{GED}(P_{\mathcal{Y}}, P_{\hat{\mathcal{Y}}}) &= \mathbb{E}_{\mathbf{y}, \mathbf{y}' \sim P_{\mathcal{Y}}} [k(\mathbf{y}, \mathbf{y}')] \\ &+ \mathbb{E}_{\hat{\mathbf{y}}, \hat{\mathbf{y}}' \sim P_{\hat{\mathcal{Y}}}} [k(\hat{\mathbf{y}}, \hat{\mathbf{y}}')] \\ &- 2 \cdot \mathbb{E}_{\mathbf{y} \sim P_{\mathcal{Y}}} \mathbb{E}_{\hat{\mathbf{y}} \sim P_{\hat{\mathcal{Y}}}} [k(\mathbf{y}, \hat{\mathbf{y}})], \end{aligned} \quad (37)$$

with marginals $P_{\mathcal{Y}}$ and $P_{\hat{\mathcal{Y}}}$, representing the true and predictive segmentation distribution, and a distance represented by kernel $k : \mathcal{Y} \times \mathcal{Y} \rightarrow \mathbb{R}$, usually the (1–IoU) or (1–Dice) score (squared by the GED). An alternative metric known as Hungarian Matching (HM) compares the predictions against the ground-truth labels through a cost matrix [74]. Subsequently, the unique optimal coupling between the two sets that minimize the average cost is determined through a combinatorial optimization algorithm. This can be also formally denoted as finding the permutation matrix \mathbf{P} , subject to the objective

$$\text{HM}(\mathcal{Y}, \hat{\mathcal{Y}}) = \frac{1}{N^2} \min_{\mathbf{P}} \text{Tr}(\mathbf{P}\mathbf{M}), \quad (36)$$

where the elements of \mathbf{M} are $M_{i,j} = k(\mathcal{Y}_i, \hat{\mathcal{Y}}_j)$, and N^2 represents the number of elements within the matrix.

For accurate comparison and evaluation of the problem, benchmarking is often constrained to publicly available multi-annotated data. For example, the Lung Image Database Consortium and Image Database Resource Initiative (LIDC-IDRI) [131] contains manually annotated lesions from lung patients and is one of the few datasets that has extensively been evaluated with appropriate metrics (see Table I). Multiple versions have been used, either with 15,096 (LIDCv1) or 12,816 (LIDCv2) patches. LIDCv1 is employed with a 60:20:20 split, while for LIDCv2 this is 70:15:15 for train:validation:test. LIDCv2 has also been used with threefold cross-validation (LIDCv2-cv), with either a 90:10 or 80:20 train:test split [59], [63], [73].

Other less commonly employed datasets include the CityScapes [132] dataset, which contains street-view images of German cities from the perspective of a driving car, have been used to artificially create class-level label ambiguity [69], [74], [81]. Classes are switched to an arbitrary auxiliary class with some probability p . Since the underlying probabilities are known, the empirical fraction of the classes from the model

TABLE I
COMPARISON OF TEST EVALUATIONS ON TWO VERSIONS OF THE LIDC-IDRI DATASET. TABLE ADAPTED FROM [95].

Method	LIDCv1		LIDCv2	
	GED ₁₆	HM-IoU ₁₆	GED ₁₆	HM-IoU ₁₆
PU-Net [69], 2018	0.310 ± 0.010	0.552 ± 0.000	0.320 ± 0.030	0.500 ± 0.030
HPU-Net [74], 2019	0.270 ± 0.010	0.530 ± 0.010	0.270 ± 0.010	0.530 ± 0.010
PhiSeg [75], 2019	0.262 ± 0.000	0.586 ± 0.000	-	-
SSN [50], 2020	0.259 ± 0.000	0.558 ± 0.000	-	-
CAR [56], 2021	-	-	0.264 ± 0.002	0.592 ± 0.005
JProb. U-Net [135], 2022	-	-	0.262 ± 0.000	0.585 ± 0.000
PixelSeg [53], 2022	0.243 ± 0.010	0.614 ± 0.000	0.260 ± 0.000	0.587 ± 0.010
MoSE [81], 2022	0.218 ± 0.001	0.624 ± 0.004	-	-
AB [136], 2022	0.213 ± 0.001	0.614 ± 0.001	-	-
CIMD [96], 2023	0.234 ± 0.005	0.587 ± 0.001	-	-
CCDM [95], 2023	0.212 ± 0.002	0.623 ± 0.002	0.239 ± 0.003	0.598 ± 0.001

predictions can be directly compared to the ground-truth values of p . Furthermore, the QUBIQ Challenge [133] contains MRI and CT data from varying organs. Also, the retinal fundus images for glaucoma analysis (RIGA) [134] dataset contains delineations of optic cup and disc boundaries by 6 experienced ophthalmologists.

Explicitly modeling the annotator distribution has been explored with an MoE approach (Section V-C), using data with consistent image-annotation pairs, provided that annotators have an intrinsically associated expertise [137]. Nevertheless, relying on the model to infer ambiguity in the parameters by observing the data, can become quite burdensome. Hence, it can be much simpler to directly model the empirical stochasticity in the annotations, which has been extensively explored in modalities such as Lung nodule detection in 2D [50], [59], [60], [62], [68], [69], [73]–[75], [138], [139], as well as 3D [79], [140], [141], Brain Tumor [50], [94], [96], [98], [142], White Matter Hyperintensities [143], Pulmonary Tumour Growth [144], Prostate [76], [145] and vascular [146], street scene [74], [95], [147], aerial imaging [101], optic cup [99], [148], abdominal multi-organ [100] and nuclei microscopy [97] segmentation. The overwhelming majority of research for this particular application has been executed with variants of conditional VAEs [59], [60], [62], [68], [69], [73]–[76], [79], [139]–[142], [144]–[146], [149], [150]. More recently, the growing popularity of DDPMs is apparent in the field [94]–[96], [98], [101]. Also, GAN-based approaches have been employed [56].

B. Model introspection

The uncertainties obtained from probabilistic models can provide an insight into the reliability of a model when the correlation between uncertainty and model accuracy is strong. This relationship has been formalized by Mukhoti *et al.* [151] through two conditional likelihoods. Firstly, the accuracy given a certain prediction, $p(A|C)$, and secondly, the uncertainty given an inaccurate prediction $p(U|I)$. Given a threshold u_T that distinguishes certain from uncertain pixels or patches, we can define pixels that are accurate and certain, accurate and uncertain, inaccurate and certain, inaccurate and uncertain, denoted by u_{ac} , u_{au} , u_{ic} , u_{iu} , respectively. Consequently, the authors combine $p(A|C) = n_{ac}/(n_{ac} + n_{au})$ and $p(U|I) = n_{ic}/(n_{ic} + n_{iu})$ to obtain the Patch Accuracy vs Patch Un-

certainty (PAvPU) metric, defined as

$$\text{PAvPU} = \frac{n_{ac} + n_{au}}{n_{ac} + n_{au} + n_{ic} + n_{iu}}. \quad (37)$$

This application has been applied in combination with MC dropout to model (video) street scenes [152], [153], remote sensing [154], [155], instance segmentation of various objects [156], point-cloud indoor scenes [157], brain [17], [158]–[163], Multiple Sclerosis [164], cardiac [165], [166], heart ventricle [163], prostate [163], carotid artery [167], lumbo-sacral [19] MRI, and Optical Coherence Tomography [168], [169], skin imaging [170], [171], lung [171] and liver CT [172] and MRI [173], and ultrasound [125], [174]. Concrete dropout has been applied to instance segmentation of *C. elegans* assays [175] and street-scenes [151]. To a lesser degree, ensembling [125], [176], Variational Inference both in 2D [177], [178] and 3D [179], M-heads (auxiliary networks) [14], [180], [181], and test-time augmentation [125] have also been used to quantify the uncertainty for quality assessment.

It can be noted that uncertainty is usually only obtained on pixel basis, while crucial information can be present in structural statistics. Hence, the Coefficient of Variation (CV) addresses this by measuring structural uncertainty through dividing the volume variance over the mean for all samples. Also, Roy *et al.* [162] propose to evaluate structural uncertainties by assuming predictions to be thresholded to binary masks with some function t , to determine the pair-wise average overlap between all respective samples as

$$\bar{D} = \mathbb{E}_{p_{\mathbf{Y}|\mathbf{X}^*}} [\text{Dice}(t(\mathbf{y}_i), t(\mathbf{y}_j))] \quad \forall i \neq j. \quad (38)$$

Finally, including information on localized uncertainty to the training objective has shown to improve generalization capabilities [182]–[185]. Note that using uncertainty to guide model training is closely related to Active Learning, which is discussed in Section VI-D.

C. Model generalization

As mentioned earlier in Section V-A, sampling new parameter permutations often improves segmentation performance, due to the model combining effect. For instance, dropout layers at the deeper decomposition levels of the SegNet [4] improves model performance [152]. Literature also reports improved performance with Concrete Dropout for semantic (instance) segmentation [151], [175]. This has been observed in multiple domains, including in-/outdoor scene understanding [151], [152], [181], [186], [187], brain tumor MRI [159], [161], [177], [188], Optical Coherence Tomography [168], low-dose Computed Tomography of lung nodules [189], colectoral polyps [190], cardiac MRI [18] and *C. elegans* roundworm microscopy images [175]. Ng *et al.* [18] have benchmarked multiple techniques for cardiac MRI segmentation and have found that ensembling results in the best performance improvement, while BBB is more robust to noise distortions.

Furthermore, the improved generalization from ensembling has also shown to produce more calibrated outputs [163]. In other work, orthogonality within and across convolutional filters of the ensemble is enforced through minimizing their cosine similarity, which reaped similar merits [49]. Nonetheless,

individual models in conventional ensembles receive data in an unstructured manner. However, it is also possible to assign specific subsets of the data to particular models (so-called ‘experts’) in the ensemble [128], commonly referred to as a Mixture of Experts (MoE). While MoE resembles ensembling in many ways, the approach additionally relies on a learnable gate that inherits the decision-taking logic. Pavlitskaya *et al.* [181] show merits of such approach for urban outdoor scene segmentation. For optic cup segmentation, Ji *et al.* [137] also condition on a normalized *expertness* vector, where each element corresponds to the weight given to a particular expert, and is inserted at the deepest layer of a U-Net. Gao *et al.* [81] have introduced a Mixture of Stochastic Experts (MoSe), which can be regarded as a stochastic adaptation of the MoE approach. Nevertheless, the methodology addresses aleatoric uncertainty quantification and has hence been discussed in Section IV-B2d.

D. Active Learning

The field of active learning [191], [192] aims to reduce the costly annotation procedure by careful selection of unlabeled training samples. A wide range of methodologies exist, but since the nature of this problem involves identifying and reducing model ignorance, the quantification of epistemic uncertainty is most appropriate. In terms of metrics, the expected increase in posterior entropy, defined by

$$H[\boldsymbol{\theta}|\mathcal{D}] - \mathbb{E}_{p(\mathbf{Y}|\mathbf{x}^*, \mathcal{D})} [H[\boldsymbol{\theta}|\mathbf{y}, \mathbf{x}^*, \mathcal{D}]], \quad (39)$$

can provide a notion to describe information gain, and thus the decrease of uncertainty for specific datapoints. Notably, minimizing the expected increase in posterior entropy is equivalent to maximizing the mutual information between the data and model parameters. This enables reformulation in terms of the output space, rather than the complex parameter space and is known as Bayesian Active Learning by Disagreement (BALD) [193], denoted as

$$\begin{aligned} I(\mathbf{y}, \boldsymbol{\theta}|\mathbf{x}^*, \mathcal{D}) &= H[\mathbf{y}|\mathbf{x}^*, \mathcal{D}] - H[\mathbf{y}|\boldsymbol{\theta}, \mathbf{x}^*, \mathcal{D}] \\ &= H[\mathbf{y}|\mathbf{x}^*, \mathcal{D}] - \mathbb{E}_{q(\boldsymbol{\theta}|\mathcal{D})} [H[\mathbf{y}|\mathbf{x}^*, \boldsymbol{\theta}]]. \end{aligned} \quad (41)$$

Active Learning through uncertainty quantification has been beneficial for medical [194]–[201], multi-view [202], remote sensing [203], street-views [204] and 3D point-cloud data [205]. These works mostly utilize MC Dropout to obtain a notion of uncertainty, but explicit VI together with BALD [185] and novel temporal-ensembling methods [206] have also been used to reduce the required human labeling. Some methods extend beyond pixel-level uncertainty, incorporating boundary information in the uncertainty quantification process [200], [204]. For example, Kasarla *et al.* [204] make use of both image and pixel-level uncertainty. Furthermore, pixels are weighed by their closeness to edges, as boundary cases are more likely to be uncertain. Similarly, Ma *et al.* [200] combine target and boundary-based uncertainty sampling, thereby ensuring diversity, effective and balanced utilization of the available information.

TABLE II
COMPARISON BETWEEN MODELS THAT QUANTIFY ALEATORIC
UNCERTAINTY.

Method	Advantages	Disadvantages	Examples
TTA	Model agnostic, no additional training parameters	Implicit likelihoods	[103]–[106]
SSN	Model agnostic, explicit likelihoods, fast sampling	Unstable training	[50]
PixelCNN	Explicit, exact likelihoods	Sequential sampling, memory intensive	[53]
GAN	Fast sampling, flexible	Unstable training, poorly defined objective, implicit likelihoods	[56], [57]
VAE	Fast sampling, flexible, interpretable latent space, ELBO	Mode/posterior collapse, amortization gap	[59]–[62], [68], [69], [73]–[75], [81], [89], [135], [141]
DDPM	Flexible, expressive	Sequential sampling	[94]–[101]

VII. DISCUSSION

This section highlights the main trends and discussion points in the field. The challenges and limitations related to the methods (Section VII-A) and downstream applications (Section VII-B) are discussed. Based on these observations, recommendations for future work will be provided in Section VII-C.

A. Discussion on methods

The core challenges with modeling segmentation distributions entails obtaining calibrated uncertainty estimates and secondly, designing spatial coherence between pixels of the samples. While the former can be achieved with conventional CNN models, the latter requires modeling correlation across pixels of the segmentation mask. As discussed in earlier sections, the desired nature of the uncertainty estimates governs the required methodology. Similarly, our discussion will follow a comparable format as the preceding sections, i.e. the aleatoric and epistemic approaches will initially be treated in a separate manner.

1) *Aleatoric methods*: The literature overview indicates that three distinct routes can be taken to model the correlation. The first method is to model the correlation directly in the pixel space. The second method entails using latent-variable modeling, where the correlation is encoded in the latent space. Finally, TTA is a more straightforward and practical approach to obtain uncertainty and requires the least modifications to existing models. We will discuss the strengths and weaknesses of each of those approaches. A summary of this is presented in Table II.

Known for its flexibility to various datasets, fast sampling time and the interpretable latent space, VAEs seem to be the most popular choice for aleatoric uncertainty quantification. Nonetheless, the shortcomings of VAEs are well known. For example, such models suffer from inference suboptimality related to ELBO optimization [65], [207] and literature on the VAE-based PU-Net often describe behavior similar to the well-known phenomena of *model collapse* [63], [68], [73]. This has been hypothesized to be caused by excessively strong decoders [64] and is especially apparent when dealing with complex hierarchical decoding structures, where additional

modifications such as the GECO objective [74], residual connections [74], [75], or deep supervision [75] are required for generalization. A unique benefit of this approach is the ability to semantically interpret the latent space with, for example, interpolation between annotation styles or the exploration of low-likelihood regions. Hence, VAE-based models serve as good choice for the task given their shortcomings are sufficiently addressed and partially solved.

Compared to the VAE-based models, the adoption of DDPMs is rather limited. This is regardless of the fact that it outperforms the VAE-based methods. Besides the point that DDPMs emerged much later in the field, their crucial limitation, similar to the PixelCNN [53], is the tedious sequential inference procedure [92], [208], [209]. This shortcoming is exacerbated in supervised settings, which often require validation through sampling on a separate data split. Regardless of these shortcomings, DDPMs are extremely flexible and avoid loss of crucial high-frequency information often found in latent-variable modeling with dimensionality reduction (e.g. blurry reconstructions of VAEs). Furthermore, it can be noted that the best-performing DDPM models are discrete in nature. While it is debatable whether shifting to categorical distributions is required for complex image generation [136], this observation implies the need for further investigation of the merits of categorical distributions in segmentation settings. Visually, this can be already quite apparent for the multi-class case, where the transition to noise is visually more gradual in the discrete transition (see Figure 13).

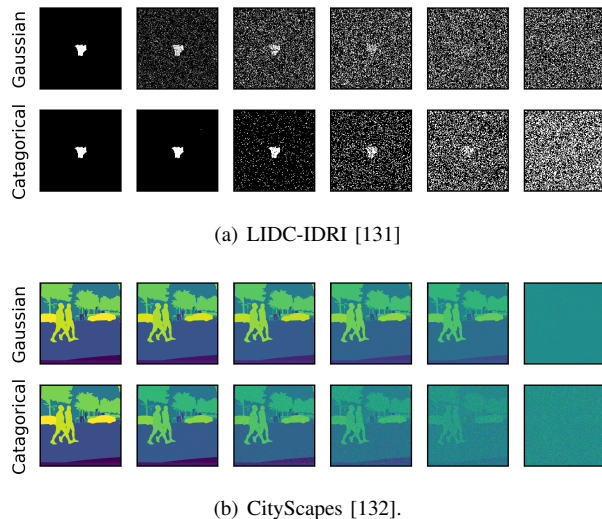


Fig. 13. Continuous vs. categorical forward diffusion process with cosine noise scheduling [210]. Note the use of categorical diffusion that results in a more gradual transition for the multi-class case.

Implicit methods such as TTA [103]–[106] have received some use in literature, but have been quickly surpassed by alternative methods. However, TTA does lead in the category of simplicity, requiring no additional mechanisms or modifications to the employed architecture. Furthermore, CAR [56] is a lesser used method and this is likely due to well-known training problems of GAN-based models [211]. Due to this, GANs require additional heuristic terms in the training

objective due to instability. For example, the training objective of CAR is a summation of four separate losses.

SSNs [50] directly model correlations in pixel space and deem simple, fast and model-agnostic modeling. Notably, SSNs also suffer from training instability due to the invertibility requirement of the covariance matrix. This can be often simply circumvented by masking out the background to avoid exploding variances and by using uncorrelated Gaussians for datapoints where the covariance matrix is singular. In practice, nevertheless, this quick-fix solution is much more frequently required than seems to be suggested, inviting further research on explicitly modeling the likelihood function in pixel space.

2) *Epistemic methods*: Almost all discussed literature quantifying epistemic uncertainty employ approximations of VI. In fact, usage of MC Dropout dominates, mainly due to it being a relatively simple, inexpensive and straightforward approach. Nevertheless, MC dropout has been subject to substantial criticism [109], [123], [212], [213]. For example, it has been shown that MC dropout can assign a probability of zero to the true posterior, which can also erroneously possess multi-modality [212]. Furthermore, MC Dropout can be heavily reliant on the interaction between model size and dropout rate, rather than the observed data [109], [213]. These weaknesses have been used as a basis for alternative techniques, where the dropout rate is learned [109], [123]. Ultimately, uncertainty from MC dropout and similar methods should be viewed as an added benefit rather than the main focus of an already functional model. If accurate uncertainty quantification is critical, MC dropout should be avoided in any case.

Finally, the optimal method for uncertainty quantification has yet to be determined. In some works, MC dropout was found to perform better than ensembling [162], [189], while in other works ensembling excels [163]. Finally, there is convincing evidence to prefer Concrete Dropout rather than MC Dropout when evaluating with the PAvPU metric [151]. All things considered, the preference for a particular methodology seems to carry a strong data-dependency [14], [125]. Our recommendation is to experiment with both explicit VI and its approximations.

B. Discussion on applications

Up until now, theoretical insights have mostly been discussed. In this section, a deeper dive is taken into the applications of uncertainty quantification. Table III provides an overview of these applications in various domains. Notably, most models are employed in healthcare use cases, where ambiguity frequently arises due to the trade-off between accuracy and the incisiveness of medical diagnosis systems. Furthermore, in the automotive industry, sensors often operate under constraints, and objects of interest are typically at a considerable distance which induces ambiguity in the acquired images. It is evident that in these fields, uncertainty is primarily utilized to quantify observer variability and/or to correlate uncertainty with prediction accuracy. Research on improved generalization and uncertainty-based active learning is much sparser. In the following sections, each respective downstream task is further discussed.

TABLE III
OVERVIEW OF DOMAINS USING UNCERTAINTY QUANTIFICATION FOR SEGMENTATION.

	Observer variability	Model Introspection	Active Learning	Model generalization
Lung	[50], [59], [60], [69], [73] [62], [68], [74], [75], [138] [79], [94], [139]–[141]	[171], [177], [189]	[182]	[189]
Brain	[50], [96], [98], [142] [94], [99], [139], [144]	[159]–[161], [163], [177]	[197]	[159], [188] [161], [177]
Outdoor scenes	[50], [74], [147] [101], [156]	[151]–[153], [157], [181]	[202], [204] [186], [187]	[151], [152], [181]
Cardiovascular		[163], [165], [166], [176] [125], [167], [178]	[194]	[214]
Prostate Prostate	[75], [76], [145] [138], [139]	[163]	[194]	
Eye	[60], [99], [100]	[168], [169]		[168]
Skin	[100]	[171], [172]	[195], [198]	
Indoor scenes	[101], [156]	[152], [157]	[202], [205]	[152]
Microscopy	[74], [97], [101]	[175], [180]		[175]
Others	[59], [73], [99], [141] [96], [139]	[19], [172]–[174], [177]	[96], [194], [200]	[190]

1) *Observer variability*: Varying delineation hypotheses present themselves as “noise” in the ground-truth of the data. This observer variability is often a result of viewing limitations and therefore heavily correlate to the input image. In turn, this explains the success of directly learning input-conditional observer variability, through explicitly modeling the likelihood distribution, rather than inferring the underlying latent parameter distribution. Nonetheless, this approach does have its limitations. For example, it has been shown that such models, without explicit conditioning, do not encapsulate more subtle variations such as distinct labeling styles [215].

A significant challenge in this domain is the lack of standardization, making benchmarking extremely difficult. The reasoning for this is twofold. Firstly, it is evident from Table III that a wide range of datasets are used in literature, often involving proprietary in-house data. This inherently makes replicating the presented results impossible. Secondly, consensus on data processing is also lacking on the publicly available datasets. For example, significant incongruity across literature is observed for the LIDC-IDRI dataset, regarding data splitting and preprocessing. Similarly, there is a lack of agreement on the implementation for the GED and HM metric. Several factors, including the kernel choice, the number of predicted samples, and the handling of empty segmentations, can significantly impact the resulting quantitative evaluations.

Regarding the evaluation metrics, we find that the literature often places excessive emphasis on improving them. This essentially forces the algorithm to predict segmentations identical to the available ground-truth masks. This can be problematic, as it defeats the original goal to predict plausible unseen segmentations, becoming a textbook case of Goodhart’s law: “When a measure becomes a target, it ceases to be a good measure”. Furthermore, the quality of the GED evaluations have been subject to substantial criticism as well [63], [74], [216]. Hence, practitioners should be extra vigilant and consider the importance to inquire domain-level experts for qualitative evaluation. Because the GED and HM are dependent on the number of segmentation masks available, an alternative is to involve additional annotators per datapoint for more accurate evaluation, but is likely to be equally expensive. This aspect calls for systematic procedures to evaluate uncertainty subject

to limited ground-truth masks.

2) **Model introspection:** Literature that evaluates models by correlating model uncertainty with error is, comparatively, much more thorough and standardized. This is especially evident by the frequent use of the PAVPU metric. Furthermore, a majority of the available research use MC Dropout and correlate the output entropy to the prediction accuracy. The disadvantage of relying on MC Dropout when the uncertainty is crucial, has been discussed in Section VII-A2. Therefore, we recommend incorporating explicit VI at specific points in the network to achieve more accurate uncertainty quantification. These points can be selected based on the layers that influence the output segmentation most significantly.

3) **Model generalization:** Epistemic uncertainty quantification methods can result in improved performance, as it often serves as a surrogate for model combination. Therefore, uncertainty quantification can be readily available in the toolbox of deep learning researchers together with other commonly used regularization techniques. In this case, simple methods such as ensembling and MC dropout, are despite their criticisms relatively harmless. Furthermore, a parallel characterization can be made with MC Dropout and placing an L_2 -norm penalty on the model weights. While this benefit is compelling, improved model performance can be also obtained with more computationally efficient regularizers. Therefore, improved performance should not be the ultimate goal of uncertainty quantification, but considered as an ancillary advantage.

4) **Active Learning:** The challenging task of Active Learning holds a significant promise and can potentially reduce the need for intensive labeling procedures, which often require specialized expertise. Furthermore, this kind of approach points towards a strong collaboration between humans (often referred to as an external *oracle*) and Artificial Intelligence, which can accelerate the adoption of such models in sectors requiring extensive specialization. Furthermore, Active Learning can accelerate privacy-centric collaboration when combined with a federated setting, enabling the active improvement of safety-critical models with human-in-the-loop intervention across local models.

However, Active Learning requires a well-generalized model using little data. This is a challenging task in the realm of deep learning-based segmentation, which usually deals with high-dimensional data and typically requires datasets of substantial size. Furthermore, many uncertainty-based approaches regularly extend conventional Active Learning for classification to segmentation by simply aggregating the pixel metrics together. For imbalanced settings, it has been shown that it can perform even worse than random selection [217]. Therefore, additional modifications such as target, boundary or diversity awareness [200], [205], or region-based annotation [204], [218] are often required to apply Active Learning to segmentation tasks.

C. Future work

In this penultimate section, we will provide recommendations for future work.

1) **Exploring generative models:** Generative modeling, a rapidly evolving field, has successfully been employed for quantifying observer variability. The benefits of quickly applying its developments to segmentation problems have been evident with state-of-the-art DDPMs [90], which were initially proposed for unsupervised image generation. Also, literature on unsupervised VAEs have greatly benefited the PU-Net [63], [68], [73]. Therefore, we advocate for a deeper contextualization of contemporary generative modeling research within probabilistic segmentation models. In fact, any unsupervised generative model can be theoretically translated to the supervised setting through intricate conditioning and can be therefore used as a probabilistic segmentation model.

Given this flexibility, it remains unclear why Normalizing Flows (NFs) remain underutilized for this task. Specifically continuous NFs, which approximate the time-dependent score function, strongly resemble DDPMs which have been extensively used for segmentation problems. Furthermore, NFs enable explicit and exact evaluation of the likelihood, which can aid in further interpretation of model predictions. Instead of modeling an iterative stochastic linear Gaussian process, NFs construct a series of invertible functions towards an isotropic Gaussian, so that inference times are therefore much faster. However, it should be noted that the invertibility constraint greatly hinders the expressiveness of intermediate functions, leading to memory-intensive architectures.

2) **Variational Inference and beyond:** A valuable contribution to the field pertains a comprehensive benchmark paper, which compares all available epistemic uncertainty quantification methods across a wide range of datasets. In particular, such study can elucidate the data-dependent preference for specific methodologies (i.e. why ensembling or MC Dropout is often preferred over explicit VI). Additionally, recent studies have shown the benefits of moving from a few large, to many small experts when using an MoE ensemble (see Section V-C) for language modeling [219]. Future work should also experiment with this.

Approaches besides VI, such as Markov Chain Monte Carlo (MCMC) or Laplace Approximations, are also viable options to approximate the Bayesian posterior. Especially the Laplace Approximation can be very beneficial, as it is easily applicable to pretrained networks. Notably, both Laplace Approximation and VI are biased and operate in the neighborhood of a single mode, while MCMC methods are a more attractive option when expecting to fit multi-modal parameter distributions. To the best of our knowledge, these approaches have not been studied within the context of uncertainty quantification in segmentation.

3) **Single-pass uncertainty:** The multiple forward passes required in many Bayesian uncertainty quantification can incur cumbersome additional costs. Hence, considerable efforts have been made towards deterministic uncertainty models [220]–[222], which only depend on a single forward pass. Mukhoti *et al.* [220] show that Gaussian Discriminant Analysis after training with SoftMax predictive distribution can in some instances surpass methods such as MC Dropout and ensembling. This approach achieves faster computation, while also providing both epistemic and aleatoric uncertainty.

Along similar lines, Evidential Deep Learning also possesses the advantage of quantifying both uncertainties with a single forward pass. This framework is based on a generalization of Bayes theorem, known as the Dempster-Shafer Theory of Evidence (DST) [223]. While common in Bayesian probability, DST does not require prior probabilities and bases subjective probabilities on belief masses assigned on a frame of discernment, i.e. the set of all possible outcomes. The use of Evidential Deep Learning has seen success in conventional classification problems [224], and Ancha *et al.* [225] recently applied this concept to segmentation to decouple aleatoric and epistemic uncertainty within a single model. Unfortunately, further research has not been published beyond this.

4) **Improved CNN architectures:** With the introduction of Vision Transformers [226], CNN-based models have been challenged in the task of semantic segmentation [227]–[229]. Regardless the success of Vision Transformers across many domains, it is clear that CNN-based encoder-decoder models such as the U-Net, remain the preferred backbone architecture [39]. This is mainly because CNNs already possess desirable inductive biases, while Transformers conversely require extensive pretraining with large datasets [230]. Nonetheless, CNNs have benefited from the recent developments in Transformers. For instance, “ConvNext” takes inspiration from contemporary Transformers to modernize existing ResNet-based CNNs, retaining the inductive biases of convolutional filters and achieving significant performance gains [231]. Since many innovations in this field focus on the technique of uncertainty quantification, the applied backbones receive less attention and might gradually become outdated. Our recommendation suggests improving current models with developments in generic CNN-based architectures.

5) **Distributing-free modeling:** A distribution-free framework known as Conformal Deep Learning, produces prediction sets that guarantee to contain the ground truth with a user-defined probability. With the help of an additional calibration set, a heuristic notion of ambiguity (i.e. miscalibrated softmax outputs) is transformed to rigorous uncertainty. This technique is especially renown for being model-agnostic, simple and highly flexible [232]. Quite recently, Conformal Prediction has been applied to segmentation problems [233]–[236], thereby enjoying the aforementioned benefits and showing an increased traction of this framework. We recommend further research in this direction to discover novel applications and benchmark against current architectures.

6) **Volumetric segmentation:** In many clinical datasets, the volumetric data are in most instances sliced to patches and processed with conventional 2D-based CNN-models. However, such models are often straightforward extensions of existing 2D models (and almost exclusively VAE-based), rarely addressing novel challenges introduced with additional dimensionalities. For example, 3D extensions of the PU-Net simply remain to use similar techniques for inserting latent samples in the decoding networks. Also, we have noted that works related to 3D BNN training require group normalization and KL-annealing for accurate generalization [179]. Therefore, general guidelines related to translating 2D segmentation models to 3D can be of great benefit for practitioners considering to

implement models for volumetric segmentations problems.

Furthermore, methodologies need to be developed in order to appropriately compare 2D to 3D models. For example, the GED cannot be estimated volumetrically with 2D models. Moreover, translating the already computation-intensive models (e.g. based on DDPMs or PixelCNNs) to 3D is another challenge, due to the memory requirement involved with volumetric data, which will increase the training load and inference time even further. Fortunately, research dedicated to volumetric segmentation is prevalent and its successes underline the need of more investigation related to 3D uncertainty quantification, that more closely aligns with real-world clinical practice and therefore encourages faster adoption.

VIII. CONCLUSION

Modeling the uncertainty of segmentation models is essential for accurately assessing the reliability in their predictions. With the vast body of literature, encompassing diverse applications and modalities, the need for a comprehensive and systematic overview of the field is addressed. We present clear definitions and unified notation of methodologies that attempt uncertainty modeling, by considering the field from a theoretical perspective. Aleatoric uncertainty can be modeled in pixel or latent space with generative models, or implicitly be expressed with test-time augmentation. Epistemic uncertainty is captured with Variational Inference on the parameter distribution, or approximated with Monte Carlo Dropout or model ensembling. Our findings show that both aleatoric and epistemic uncertainty modeling enable the practice of four distinct downstream tasks, which enable to highlight the main challenges and limitations of current work, both related to the theoretical frameworks and to the real-world applications.

Our future recommendations pertain aligning the field with advancements in general generative modeling and Deep Learning architectures. Furthermore, the adoption of deterministic uncertainty quantification methods that avoid multiple forward passes, such as Conformal and Evidential Deep Learning, are suggested. Particularly the latter approach is interesting due to its ability to incorporate both uncertainty types. Since most epistemic uncertainty quantification is performed with approximate Variational Inference, a comprehensive benchmark study of these techniques, as well as exploration of other techniques such as Markov Chain Monte Carlo (MCMC) or Laplace Approximation, is a beneficial contribution to the field. Finally, due to the clinical relevance of uncertainty in semantic segmentation, more attention is advised to models catering to volumetric data. In this manner, the review paper guides researchers on the topic of probabilistic segmentation and suggests future endeavors within the lightning-fast evolving field of Deep Learning-based Computer Vision.

REFERENCES

- [1] R. Szeliski, “Computer vision - algorithms and applications,” in *Texts in Computer Science*, 2010.
- [2] O. Ronneberger, P. Fischer, and T. Brox, “U-net: Convolutional networks for biomedical image segmentation,” in *MICCAI*, ser. LNCS, vol. 9351. Springer, 2015, pp. 234–241.
- [3] E. Shelhamer, J. Long, and T. Darrell, “Fully convolutional networks for semantic segmentation,” *IEEE/CVF CVPR*, pp. 3431–3440, 2014.

- [4] V. Badrinarayanan, A. Kendall, and R. Cipolla, "Segnet: A deep convolutional encoder-decoder architecture for image segmentation," *IEEE Trans. Pattern Anal. Mach. Intell.*, vol. 39, pp. 2481–2495, 2015.
- [5] T.-Y. Lin, M. Maire, S. J. Belongie, J. Hays, P. Perona, D. Ramanan, P. Dollár, and C. L. Zitnick, "Microsoft coco: Common objects in context," in *ECCV*, 2014.
- [6] M. Cordts, M. Omran, S. Ramos, T. Rehfeld, M. Enzweiler, R. Benenson, U. Franke, S. Roth, and B. Schiele, "The Cityscapes Dataset for Semantic Urban Scene Understanding," Apr. 2016, arXiv:1604.01685 [cs].
- [7] S. R. Richter, V. Vineet, S. Roth, and V. Koltun, "Playing for data: Ground truth from computer games," *ArXiv*, vol. abs/1608.02192, 2016.
- [8] C. Blundell, J. Cornebise, K. Kavukcuoglu, and D. Wierstra, "Weight uncertainty in neural network," in *ICML*. PMLR, 2015, pp. 1613–1622.
- [9] C. Guo, G. Pleiss, Y. Sun, and K. Q. Weinberger, "On calibration of modern neural networks," in *ICML*. PMLR, 2017, pp. 1321–1330.
- [10] D. P. Kingma and M. Welling, "Auto-encoding variational bayes," *arXiv preprint arXiv:1312.6114*, 2013.
- [11] A. Kendall and Y. Gal, "What uncertainties do we need in bayesian deep learning for computer vision?" in *NeurIPS*, 2017.
- [12] E. Hüllermeier and W. Waegeman, "Aleatoric and epistemic uncertainty in machine learning: An introduction to concepts and methods," *Machine Learning*, vol. 110, pp. 457–506, 2021.
- [13] A. Der Kiureghian and O. Ditlevsen, "Aleatory or epistemic? does it matter?" *Structural safety*, vol. 31, no. 2, pp. 105–112, 2009.
- [14] A. Jungo and M. Reyes, "Assessing reliability and challenges of uncertainty estimations for medical image segmentation," in *MICCAI*. Springer, 2019, pp. 48–56.
- [15] Y. Kwon, J.-H. Won, B. J. Kim, and M. C. Paik, "Uncertainty quantification using bayesian neural networks in classification: Application to biomedical image segmentation," *Computational Statistics & Data Analysis*, vol. 142, p. 106816, 2020.
- [16] B. McCrindle, K. Zukotynski, T. E. Doyle, and M. D. Noseworthy, "A radiology-focused review of predictive uncertainty for ai interpretability in computer-assisted segmentation," *Radiology: Artificial Intelligence*, vol. 3, no. 6, p. e210031, 2021.
- [17] A. Jungo, F. Balsiger, and M. Reyes, "Analyzing the quality and challenges of uncertainty estimations for brain tumor segmentation," *Frontiers in neuroscience*, vol. 14, p. 501743, 2020.
- [18] M. Ng, F. Guo, L. Biswas, S. E. Petersen, S. K. Piechnik, S. Neubauer, and G. Wright, "Estimating uncertainty in neural networks for cardiac mri segmentation: A benchmark study," *IEEE Trans. Biomed. Eng.*, 2022.
- [19] P. Roshanzamir, H. Rivaz, J. Ahn, H. Mirza, N. Naghdi, M. Anstruther, M. C. Battié, M. Fortin, and Y. Xiao, "How inter-rater variability relates to aleatoric and epistemic uncertainty: a case study with deep learning-based paraspinal muscle segmentation," in *UNSURE workshop, MICCAI*. Springer, 2023, pp. 74–83.
- [20] S. Minaee, Y. Boykov, F. M. Porikli, A. J. Plaza, N. Kehtarnavaz, and D. Terzopoulos, "Image segmentation using deep learning: A survey," *IEEE Trans. Pattern Anal. Mach. Intell.*, vol. 44, pp. 3523–3542, 2020.
- [21] N. Otsu, "A threshold selection method from gray level histograms," *IEEE Transactions on Systems, Man, and Cybernetics*, vol. 9, pp. 62–66, 1979.
- [22] N. Dhanachandra, K. Mangle, and Y. J. Chanu, "Image segmentation using k -means clustering algorithm and subtractive clustering algorithm," *Procedia Computer Science*, vol. 54, pp. 764–771, 2015.
- [23] R. Nock and F. Nielsen, "Statistical region merging," *IEEE Trans. Pattern Anal. Mach. Intell.*, vol. 26, pp. 1452–1458, 2004.
- [24] L. Najman and M. Schmitt, "Watershed of a continuous function," *Signal Process.*, vol. 38, pp. 99–112, 1994.
- [25] M. Kass, A. P. Witkin, and D. Terzopoulos, "Snakes: Active contour models," *IJCV*, vol. 1, pp. 321–331, 2004.
- [26] Y. Boykov, O. Veksler, and R. Zabih, "Fast approximate energy minimization via graph cuts," *IEEE ICCV*, vol. 1, pp. 377–384 vol.1, 2001.
- [27] N. Plath, M. Toussaint, and S. Nakajima, "Multi-class image segmentation using conditional random fields and global classification," in *ICML*, 2009.
- [28] J.-L. Starck, M. Elad, and D. L. Donoho, "Image decomposition via the combination of sparse representations and a variational approach," *IEEE IEEE Trans. Image Process.*, vol. 14, pp. 1570–1582, 2005.
- [29] S. Minaee and Y. Wang, "An admm approach to masked signal decomposition using subspace representation," *IEEE IEEE Trans. Image Process.*, vol. 28, pp. 3192–3204, 2017.
- [30] Y. LeCun, L. Bottou, Y. Bengio, and P. Haffner, "Gradient-based learning applied to document recognition," *Proceedings of the IEEE*, vol. 86, no. 11, pp. 2278–2324, 1998.
- [31] A. Krizhevsky, I. Sutskever, and G. E. Hinton, "Imagenet classification with deep convolutional neural networks," *NeurIPS*, vol. 25, 2012.
- [32] K. Simonyan and A. Zisserman, "Very deep convolutional networks for large-scale image recognition," *arXiv preprint arXiv:1409.1556*, 2014.
- [33] C. Szegedy, W. Liu, Y. Jia, P. Sermanet, S. Reed, D. Anguelov, D. Erhan, V. Vanhoucke, and A. Rabinovich, "Going deeper with convolutions (2014)," *arXiv preprint arXiv:1409.4842*, vol. 10, 2014.
- [34] L.-C. Chen, G. Papandreou, F. Schroff, and H. Adam, "Rethinking atrous convolution for semantic image segmentation," *arXiv preprint arXiv:1706.05587*, 2017.
- [35] A. Howard, M. Sandler, G. Chu, L.-C. Chen, B. Chen, M. Tan, W. Wang, Y. Zhu, R. Pang, V. Vasudevan *et al.*, "Searching for mobilenetv3," in *IEEE/CVF ICCV*, 2019, pp. 1314–1324.
- [36] H. Noh, S. Hong, and B. Han, "Learning deconvolution network for semantic segmentation," *IEEE ICCV*, pp. 1520–1528, 2015.
- [37] Y. Yuan, X. Chen, and J. Wang, "Object-contextual representations for semantic segmentation," in *ECCV*, 2019.
- [38] F. Isensee, P. F. Jaeger, S. A. A. Kohl, J. Petersen, and K. Maier-Hein, "nnu-net: a self-configuring method for deep learning-based biomedical image segmentation," *Nature Methods*, vol. 18, pp. 203 – 211, 2020.
- [39] M. Eisenmann, A. Reinke, and V. W. *et al.*, "Why is the winner the best?" *ArXiv*, vol. abs/2303.17719, 2023.
- [40] F. Isensee, T. Wald, C. Ulrich, M. Baumgartner, S. Roy, K. Maier-Hein, and P. F. Jaeger, "nnu-net revisited: A call for rigorous validation in 3d medical image segmentation," *arXiv preprint arXiv:2404.09556*, 2024.
- [41] M. Figueiredo, "Adaptive sparseness using jeffreys prior," *NeurIPS*, vol. 14, 2001.
- [42] A. Kaban, "On bayesian classification with laplace priors," *Pattern Recognition Letters*, vol. 28, no. 10, pp. 1271–1282, 2007.
- [43] Z. Ding, X. Han, P. Liu, and M. Niethammer, "Local Temperature Scaling for Probability Calibration," Jul. 2021, arXiv:2008.05105 [cs].
- [44] J. L. Silva and A. L. Oliveira, "Using Soft Labels to Model Uncertainty in Medical Image Segmentation," Sep. 2021, arXiv:2109.12622 [cs].
- [45] B. Liu, I. B. Ayed, A. Galdran, and J. Dolz, "The Devil is in the Margin: Margin-based Label Smoothing for Network Calibration," Mar. 2022, arXiv:2111.15430 [cs].
- [46] J. Mukhoti, V. Kulharia, A. Sanyal, S. Golodetz, P. Torr, and P. Dokania, "Calibrating deep neural networks using focal loss," *NeurIPS*, vol. 33, pp. 15 288–15 299, 2020.
- [47] C. Szegedy, V. Vanhoucke, S. Ioffe, J. Shlens, and Z. Wojna, "Rethinking the inception architecture for computer vision," in *IEEE/CVF CVPR*, 2016, pp. 2818–2826.
- [48] G. Pereyra, G. Tucker, J. Chorowski, Ł. Kaiser, and G. Hinton, "Regularizing neural networks by penalizing confident output distributions," *arXiv preprint arXiv:1701.06548*, 2017.
- [49] A. Larrabazal, C. Martinez, J. Dolz, and E. Ferrante, "Maximum entropy on erroneous predictions (meep): Improving model calibration for medical image segmentation," *arXiv preprint arXiv:2112.12218*, 2021.
- [50] M. Monteiro, L. Le Folgoc, D. Coelho de Castro, N. Pawlowski, B. Marques, K. Kamnitsas, M. van der Wilk, and B. Glocker, "Stochastic Segmentation Networks: Modelling Spatially Correlated Aleatoric Uncertainty," in *NeurIPS*, vol. 33. Curran Associates, Inc., 2020, pp. 12 756–12 767.
- [51] A. Van Den Oord, N. Kalchbrenner, and K. Kavukcuoglu, "Pixel recurrent neural networks," in *ICML*. PMLR, 2016, pp. 1747–1756.
- [52] A. Van den Oord, N. Kalchbrenner, L. Espeholt, O. Vinyals, A. Graves *et al.*, "Conditional image generation with pixelcnn decoders," *NeurIPS*, vol. 29, 2016.
- [53] W. Zhang, X. Zhang, S. Huang, Y. Lu, and K. Wang, "PixelSeg: Pixel-by-Pixel Stochastic Semantic Segmentation for Ambiguous Medical Images," in *Proceedings of the 30th ACM International Conference on Multimedia*. Lisboa Portugal: ACM, Oct. 2022, pp. 4742–4750.
- [54] Y. Zheng, T. He, Y. Qiu, and D. P. Wipf, "Learning manifold dimensions with conditional variational autoencoders," *NeurIPS*, vol. 35, pp. 34 709–34 721, 2022.
- [55] I. Goodfellow, J. Pouget-Abadie, M. Mirza, B. Xu, D. Warde-Farley, S. Ozair, A. Courville, and Y. Bengio, "Generative adversarial nets," *NeurIPS*, vol. 27, 2014.
- [56] E. Kassapis, G. Dikov, D. K. Gupta, and C. Nugteren, "Calibrated Adversarial Refinement for Stochastic Semantic Segmentation," Aug. 2021, arXiv:2006.13144 [cs].

- [57] P. Isola, J.-Y. Zhu, T. Zhou, and A. A. Efros, "Image-to-image translation with conditional adversarial networks," in *IEEE/CVF CVPR*, 2017, pp. 1125–1134.
- [58] D. J. Rezende and S. Mohamed, "Variational inference with normalizing flows," *arXiv preprint arXiv:1505.05770*, 2015.
- [59] M. A. Valiuddin, C. G. Viviers, R. J. van Sloun, P. H. de With, and F. van der Sommen, "Improving aleatoric uncertainty quantification in multi-annotated medical image segmentation with normalizing flows," in *UNSURE workshop, MICCAI*. Springer, 2021, pp. 75–88.
- [60] R. Selvan, F. Faye, J. Middleton, and A. Pai, "Uncertainty quantification in medical image segmentation with normalizing flows," Aug. 2020, arXiv:2006.02683 [cs, stat].
- [61] I. Bhat, J. P. W. Pluim, M. A. Viergever, and H. J. Kuijff, "Effect of latent space distribution on the segmentation of images with multiple annotations," Apr. 2023, arXiv:2304.13476 [cs, eess].
- [62] I. Bhat, J. P. Pluim, and H. J. Kuijff, "Generalized probabilistic u-net for medical image segmentation," in *UNSURE workshop, MICCAI*. Springer, 2022, pp. 113–124.
- [63] M. M. Amaan Valiuddin, C. G. A. Viviers, R. J. G. Van Sloun, P. H. N. De With, and F. v. d. Sommen, "Investigating and improving latent density segmentation models for aleatoric uncertainty quantification in medical imaging," *IEEE Trans. Med. Imag.*, pp. 1–1, 2024.
- [64] X. Chen, D. P. Kingma, T. Salimans, Y. Duan, P. Dhariwal, J. Schulman, I. Sutskever, and P. Abbeel, "Variational lossy autoencoder," *arXiv preprint arXiv:1611.02731*, 2016.
- [65] S. Zhao, J. Song, and S. Ermon, "Infovae: Information maximizing variational autoencoders," *arXiv preprint arXiv:1706.02262*, 2017.
- [66] M. Cuturi, "Sinkhorn distances: Lightspeed computation of optimal transport," *NeurIPS*, vol. 26, 2013.
- [67] W. Zhang, X. Zhang, S. Huang, Y. Lu, and K. Wang, "A probabilistic model for controlling diversity and accuracy of ambiguous medical image segmentation," in *Proceedings of the 30th ACM International Conference on Multimedia*, 2022, pp. 4751–4759.
- [68] D. Qiu and L. M. Lui, "Modal uncertainty estimation via discrete latent representation," *arXiv preprint arXiv:2007.12858*, 2020.
- [69] S. A. A. Kohl, B. Romera-Paredes, C. Meyer, J. De Fauw, J. R. Ledsam, K. H. Maier-Hein, S. M. A. Eslami, D. J. Rezende, and O. Ronneberger, "A Probabilistic U-Net for Segmentation of Ambiguous Images," Jan. 2019, arXiv:1806.05034 [cs, stat].
- [70] O. Bousquet, S. Gelly, I. Tolstikhin, C.-J. Simon-Gabriel, and B. Schoelkopf, "From optimal transport to generative modeling: the vegan cookbook," *arXiv preprint arXiv:1705.07642*, 2017.
- [71] I. Higgins, L. Matthey, A. Pal, C. P. Burgess, X. Glorot, M. M. Botvinick, S. Mohamed, and A. Lerchner, "beta-vae: Learning basic visual concepts with a constrained variational framework." *ICLR (Poster)*, vol. 3, 2017.
- [72] A. Van Den Oord, O. Vinyals *et al.*, "Neural discrete representation learning," *NeurIPS*, vol. 30, 2017.
- [73] A. Valiuddin, C. Viviers, R. van Sloun, P. de With, and F. van der Sommen, "Retaining informative latent variables in probabilistic segmentation," in *IEEE ICASSP*. IEEE, 2024, pp. 5635–5639.
- [74] S. A. A. Kohl, B. Romera-Paredes, K. H. Maier-Hein, D. J. Rezende, S. M. A. Eslami, P. Kohli, A. Zisserman, and O. Ronneberger, "A Hierarchical Probabilistic U-Net for Modeling Multi-Scale Ambiguities," May 2019, arXiv:1905.13077 [cs].
- [75] C. F. Baumgartner, K. C. Tezcan, K. Chaitanya, A. M. Hötter, U. J. Muehlematter, K. Schawkat, A. S. Becker, O. Donati, and E. Konukoglu, "Phiseg: Capturing uncertainty in medical image segmentation," in *MICCAI*. Springer, 2019, pp. 119–127.
- [76] A. Saha, J. Bosma, J. Linmans, M. Hosseinzadeh, and H. Huisman, "Anatomical and Diagnostic Bayesian Segmentation in Prostate MRI S-S\$Should Different Clinical Objectives Mandate Different Loss Functions?" Oct. 2021, arXiv:2110.12889 [cs, eess].
- [77] A. Saha, M. Hosseinzadeh, and H. Huisman, "Encoding clinical priori in 3d convolutional neural networks for prostate cancer detection in bpmri," *arXiv preprint arXiv:2011.00263*, 2020.
- [78] C. G. Viviers, M. A. Valiuddin, F. van der Sommen *et al.*, "Probabilistic 3d segmentation for aleatoric uncertainty quantification in full 3d medical data," in *Medical Imaging 2023: Computer-Aided Diagnosis*, vol. 12465. SPIE, 2023, pp. 341–351.
- [79] E. Chotzoglou and B. Kainz, "Exploring the relationship between segmentation uncertainty, segmentation performance and inter-observer variability with probabilistic networks," in *LABELS, MICCAI*. Springer, 2019, pp. 51–60.
- [80] X. Long, W. Chen, Q. Wang, X. Zhang, C. Liu, Y. Li, and J. Zhang, "A probabilistic model for segmentation of ambiguous 3d lung nodule," in *IEEE ICASSP*. IEEE, 2021, pp. 1130–1134.
- [81] Z. Gao, Y. Chen, C. Zhang, and X. He, "Modeling multimodal aleatoric uncertainty in segmentation with mixture of stochastic expert," *arXiv preprint arXiv:2212.07328*, 2022.
- [82] C. K. Sønderby, T. Raiko, L. Maaløe, S. K. Sønderby, and O. Winther, "Ladder variational autoencoders," *NeurIPS*, vol. 29, 2016.
- [83] D. P. Kingma, T. Salimans, R. Jozefowicz, X. Chen, I. Sutskever, and M. Welling, "Improved variational inference with inverse autoregressive flow," *NeurIPS*, vol. 29, 2016.
- [84] A. Klushyn, N. Chen, R. Kurle, B. Cseke, and P. van der Smagt, "Learning hierarchical priors in vaes," *NeurIPS*, vol. 32, 2019.
- [85] K. Gregor, I. Danihelka, A. Graves, D. Rezende, and D. Wierstra, "Draw: A recurrent neural network for image generation," in *ICML*. PMLR, 2015, pp. 1462–1471.
- [86] R. Ranganath, D. Tran, and D. Blei, "Hierarchical variational models," in *ICML*. PMLR, 2016, pp. 324–333.
- [87] E. Jang, S. Gu, and B. Poole, "Categorical reparameterization with gumbel-softmax," *arXiv preprint arXiv:1611.01144*, 2016.
- [88] I. A. Huijben, W. Kool, M. B. Paulus, and R. J. Van Sloun, "A review of the gumbel-max trick and its extensions for discrete stochasticity in machine learning," *IEEE Trans. Pattern Anal. Mach. Intell.*, vol. 45, no. 2, pp. 1353–1371, 2022.
- [89] A. Schmidt, P. Morales-Álvarez, and R. Molina, "Probabilistic modeling of inter- and intra-observer variability in medical image segmentation," in *IEEE/CVF ICCV*, 2023, pp. 21 097–21 106.
- [90] J. Ho, A. Jain, and P. Abbeel, "Denosing diffusion probabilistic models," *NeurIPS*, vol. 33, pp. 6840–6851, 2020.
- [91] H. Song, M. Kim, D. Park, Y. Shin, and J.-G. Lee, "Learning From Noisy Labels With Deep Neural Networks: A Survey," *IEEE Trans. Neural Netw. Learn. Syst.*, pp. 1–19, 2022.
- [92] J. Song, C. Meng, and S. Ermon, "Denosing diffusion implicit models," *arXiv preprint arXiv:2010.02502*, 2020.
- [93] C. Luo, "Understanding diffusion models: A unified perspective," *arXiv preprint arXiv:2208.11970*, 2022.
- [94] T. Chen, C. Wang, and H. Shan, "BerDiff: Conditional Bernoulli Diffusion Model for Medical Image Segmentation," Apr. 2023, arXiv:2304.04429 [cs].
- [95] L. Zbinden, L. Doorenbos, T. Pissas, A. T. Huber, R. Sznitman, and P. Márquez-Neila, "Stochastic Segmentation with Conditional Categorical Diffusion Models," Apr. 2023.
- [96] A. Rahman, J. M. J. Valanarasu, I. Hacihaliloglu, and V. M. Patel, "Ambiguous Medical Image Segmentation using Diffusion Models," Apr. 2023, arXiv:2304.04745 [cs].
- [97] L. Bogensperger, D. Narnhofer, F. Ilic, and T. Pock, "Score-Based Generative Models for Medical Image Segmentation using Signed Distance Functions," Mar. 2023, arXiv:2303.05966 [cs].
- [98] J. Wolleb, R. Sandkühler, F. Bieder, P. Valmaggia, and P. C. Cattin, "Diffusion Models for Implicit Image Segmentation Ensembles," Dec. 2021, arXiv:2112.03145 [cs].
- [99] J. Wu, R. Fu, H. Fang, Y. Zhang, Y. Yang, H. Xiong, H. Liu, and Y. Xu, "MedSegDiff: Medical Image Segmentation with Diffusion Probabilistic Model," Jan. 2023, arXiv:2211.00611 [cs].
- [100] J. Wu, R. Fu, H. Fang, Y. Zhang, and Y. Xu, "MedSegDiff-V2: Diffusion based Medical Image Segmentation with Transformer," Jan. 2023, arXiv:2301.11798 [cs, eess].
- [101] T. Amit, T. Shaharby, E. Nachmani, and L. Wolf, "Segdiff: Image segmentation with diffusion probabilistic models," *arXiv preprint arXiv:2112.00390*, 2021.
- [102] M. S. Ayhan and P. Berens, "Test-time data augmentation for estimation of heteroscedastic aleatoric uncertainty in deep neural networks," in *Medical Imaging with Deep Learning*, 2022.
- [103] G. Wang, W. Li, M. Aertsen, J. Deprest, S. Ourselin, and T. Vercauteren, "Aleatoric uncertainty estimation with test-time augmentation for medical image segmentation with convolutional neural networks," *Neurocomputing*, vol. 338, pp. 34–45, 2019.
- [104] M. Racic, H. E. Wong, J. J. G. Ortiz, B. A. Cimini, J. V. Guttag, and A. V. Dalca, "Tyche: Stochastic in-context learning for medical image segmentation," in *IEEE/CVF CVPR*, 2024, pp. 11 159–11 173.
- [105] G. Wang, W. Li, S. Ourselin, and T. Vercauteren, "Automatic brain tumor segmentation using convolutional neural networks with test-time augmentation," in *BrainLes workshop, MICCAI*. Springer, 2019, pp. 61–72.
- [106] H. Pan, Y. Feng, Q. Chen, C. Meyer, and X. Feng, "Prostate segmentation from 3d mri using a two-stage model and variable-input based uncertainty measure," in *2019 IEEE 16th International Symposium on Biomedical Imaging (ISBI 2019)*. IEEE, 2019, pp. 468–471.
- [107] R. M. Neal, *Bayesian learning for neural networks*. Springer Science & Business Media, 2012, vol. 118.

- [108] Y. Gal and Z. Ghahramani, "Dropout as a bayesian approximation: Representing model uncertainty in deep learning," in *ICML*. PMLR, 2016, pp. 1050–1059.
- [109] D. P. Kingma, T. Salimans, and M. Welling, "Variational dropout and the local reparameterization trick," *NeurIPS*, vol. 28, 2015.
- [110] B. Lakshminarayanan, A. Pritzel, and C. Blundell, "Simple and scalable predictive uncertainty estimation using deep ensembles," *NeurIPS*, vol. 30, 2017.
- [111] D. J. C. Mackay, *Bayesian methods for adaptive models*. California Institute of Technology, 1992.
- [112] A. Korattikara Balan, V. Rathod, K. P. Murphy, and M. Welling, "Bayesian dark knowledge," *NeurIPS*, vol. 28, 2015.
- [113] J. T. Springenberg, A. Klein, S. Falkner, and F. Hutter, "Bayesian optimization with robust bayesian neural networks," *NeurIPS*, vol. 29, 2016.
- [114] M. Welling and Y. W. Teh, "Bayesian learning via stochastic gradient langevin dynamics," in *ICML*, 2011, pp. 681–688.
- [115] J. M. Hernández-Lobato and R. Adams, "Probabilistic backpropagation for scalable learning of bayesian neural networks," in *ICML*. PMLR, 2015, pp. 1861–1869.
- [116] L. Hasenclever, S. Webb, T. Lienart, S. Vollmer, B. Lakshminarayanan, C. Blundell, and Y. W. Teh, "Distributed bayesian learning with stochastic natural gradient expectation propagation and the posterior server," *The Journal of Machine Learning Research*, vol. 18, no. 1, pp. 3744–3780, 2017.
- [117] C. Louizos and M. Welling, "Structured and efficient variational deep learning with matrix gaussian posteriors," in *ICML*. PMLR, 2016, pp. 1708–1716.
- [118] C. M. Bishop, *Neural networks for pattern recognition*. Oxford university press, 1995.
- [119] T. P. Minka, "Bayesian model averaging is not model combination," Available electronically at <http://www.stat.cmu.edu/minka/papers/bma.html>, pp. 1–2, 2000.
- [120] B. Clarke, "Comparing bayes model averaging and stacking when model approximation error cannot be ignored," *Journal of Machine Learning Research*, vol. 4, no. Oct, pp. 683–712, 2003.
- [121] B. Lakshminarayanan, "Decision trees and forests: a probabilistic perspective." Ph.D. dissertation, UCL (University College London), 2016.
- [122] S. Wager, S. Wang, and P. S. Liang, "Dropout training as adaptive regularization," *NeurIPS*, vol. 26, 2013.
- [123] Y. Gal, J. Hron, and A. Kendall, "Concrete dropout," *NeurIPS*, vol. 30, 2017.
- [124] C. J. Maddison, A. Mnih, and Y. W. Teh, "The concrete distribution: A continuous relaxation of discrete random variables," *arXiv preprint arXiv:1611.00712*, 2016.
- [125] L. Dahal, A. Kafle, and B. Khanal, "Uncertainty Estimation in Deep 2D Echocardiography Segmentation," May 2020, arXiv:2005.09349 [cs].
- [126] J. Xie, B. Xu, and Z. Chuang, "Horizontal and vertical ensemble with deep representation for classification," *arXiv preprint arXiv:1306.2759*, 2013.
- [127] G. Huang, Y. Li, G. Pleiss, Z. Liu, J. E. Hopcroft, and K. Q. Weinberger, "Snapshot ensembles: Train 1, get m for free," *arXiv preprint arXiv:1704.00109*, 2017.
- [128] R. A. Jacobs, M. I. Jordan, S. J. Nowlan, and G. E. Hinton, "Adaptive mixtures of local experts," *Neural computation*, vol. 3, no. 1, pp. 79–87, 1991.
- [129] J. Shawe-Taylor, "Kernel methods for pattern analysis," *Cambridge University Press google schola*, vol. 2, pp. 181–201, 2004.
- [130] A. Gretton, K. M. Borgwardt, M. J. Rasch, B. Schölkopf, and A. Smola, "A kernel two-sample test," *The Journal of Machine Learning Research*, vol. 13, no. 1, pp. 723–773, 2012.
- [131] S. G. e. Armato, "The Lung Image Database Consortium (LIDC) and Image Database Resource Initiative (IDRI): A Completed Reference Database of Lung Nodules on CT Scans: The LIDC/IDRI thoracic CT database of lung nodules," *Medical Physics*, vol. 38, no. 2, pp. 915–931, Jan. 2011.
- [132] M. Cordts, M. Omran, S. Ramos, T. Rehfeld, M. Enzweiler, R. Benenson, U. Franke, S. Roth, and B. Schiele, "The cityscapes dataset for semantic urban scene understanding," *IEEE/CVF CVPR*, pp. 3213–3223, 2016.
- [133] "QUBIQ 2021." [Online]. Available: <https://qubiq21.grand-challenge.org/QUBIQ2021/>
- [134] A. Almazroa, S. Alodhayb, E. Osman, E. Ramadan, M. Hummadi, M. Dlaim, M. Alkatee, K. Raahemifar, and V. Lakshminarayanan, "Retinal fundus images for glaucoma analysis: the riga dataset," in *Medical Imaging 2018: Imaging Informatics for Healthcare, Research, and Applications*, vol. 10579. SPIE, 2018, pp. 55–62.
- [135] W. Zhang, X. Zhang, S. Huang, Y. Lu, and K. Wang, "A Probabilistic Model for Controlling Diversity and Accuracy of Ambiguous Medical Image Segmentation," in *Proceedings of the 30th ACM International Conference on Multimedia*. Lisboa Portugal: ACM, Oct. 2022, pp. 4751–4759.
- [136] T. Chen, R. Zhang, and G. Hinton, "Analog bits: Generating discrete data using diffusion models with self-conditioning," *arXiv preprint arXiv:2208.04202*, 2022.
- [137] W. Ji, S. Yu, J. Wu, K. Ma, C. Bian, Q. Bi, J. Li, H. Liu, L. Cheng, and Y. Zheng, "Learning Calibrated Medical Image Segmentation via Multi-rater Agreement Modeling," in *2021 IEEE/CVF Conference on Computer Vision and Pattern Recognition (CVPR)*. Nashville, TN, USA: IEEE, Jun. 2021, pp. 12 336–12 346.
- [138] M. Gantenbein, E. Erdil, and E. Konukoglu, "Revphiseq: A memory-efficient neural network for uncertainty quantification in medical image segmentation," in *UNSURE workshop, MICCAI*. Springer, 2020, pp. 13–22.
- [139] Q. Hu, H. Wang, J. Luo, Y. Luo, Z. Zhanga, J. S. Kirschke, B. Wiestler, B. Menze, J. Zhang, and H. B. Li, "Inter-rater uncertainty quantification in medical image segmentation via rater-specific bayesian neural networks," *arXiv preprint arXiv:2306.16556*, 2023.
- [140] X. Long, W. Chen, Q. Wang, X. Zhang, C. Liu, Y. Li, and J. Zhang, "A Probabilistic Model for Segmentation of Ambiguous 3D Lung Nodule," in *ICASSP 2021 - 2021 IEEE International Conference on Acoustics, Speech and Signal Processing (ICASSP)*. Toronto, ON, Canada: IEEE, Jun. 2021, pp. 1130–1134.
- [141] C. Viviers, A. Valiuddin, P. H. N. De With, and F. Van Der Sommen, "Probabilistic 3D segmentation for aleatoric uncertainty quantification in full 3D medical data," in *Medical Imaging 2023: Computer-Aided Diagnosis*, K. M. Iftekharuddin and W. Chen, Eds. San Diego, United States: SPIE, Apr. 2023, p. 31.
- [142] C. Savadikar, R. Kulhalli, and B. Garware, "Brain tumour segmentation using probabilistic u-net," in *BrainLes workshop, MICCAI*. Springer, 2021, pp. 255–264.
- [143] B. Philips, M. del C. Valdes Hernandez, S. Munoz Maniega, M. E. Bastin, E. Sakka, U. Clancy, J. M. Wardlaw, and M. O. Bernabeu, "Stochastic uncertainty quantification techniques fail to account for inter-analyst variability in white matter hyperintensity segmentation," in *Annual Conference on Medical Image Understanding and Analysis*. Springer, 2024, pp. 34–53.
- [144] X. Liu, F. Xing, T. Marin, G. E. Fakhri, and J. Woo, "Variational Inference for Quantifying Inter-observer Variability in Segmentation of Anatomical Structures," Jan. 2022, arXiv:2201.07106 [cs].
- [145] A. Saha, M. Hosseinzadeh, and H. Huisman, "End-to-end prostate cancer detection in bpMRI via 3D CNNs: Effects of attention mechanisms, clinical priori and decoupled false positive reduction," *Medical Image Analysis*, vol. 73, p. 102155, Oct. 2021.
- [146] C. Viviers, M. Ramaekers, A. Valiuddin, T. Hellström, N. Tasios, J. van der Ven, I. Jacobs, L. Ewals, J. Nederend, M. Luyer *et al.*, "Segmentation-based assessment of tumor-vessel involvement for surgical resectability prediction of pancreatic ductal adenocarcinoma," in *IEEE/CVF ICCV*, 2023, pp. 2421–2431.
- [147] E. Hoozeboom, D. Nielsen, P. Jaini, P. Forré, and M. Welling, "Argmax flows and multinomial diffusion: Learning categorical distributions," *NeurIPS*, vol. 34, pp. 12 454–12 465, 2021.
- [148] A. M. Wundram, P. Fischer, S. Wunderlich, H. Faber, L. M. Koch, P. Berens, and C. F. Baumgartner, "Leveraging probabilistic segmentation models for improved glaucoma diagnosis: A clinical pipeline approach," in *Medical Imaging with Deep Learning*, 2024.
- [149] P. Fischer, K. Thomas, and C. F. Baumgartner, "Uncertainty estimation and propagation in accelerated mri reconstruction," in *UNSURE workshop, MICCAI*. Springer, 2023, pp. 84–94.
- [150] X. Rafael-Palou, A. Aubanell, M. Ceresa, V. Ribas, G. Piella, and M. A. G. Ballester, "An Uncertainty-aware Hierarchical Probabilistic Network for Early Prediction, Quantification and Segmentation of Pulmonary Tumour Growth," Apr. 2021, arXiv:2104.08789 [cs].
- [151] J. Mukhoti and Y. Gal, "Evaluating bayesian deep learning methods for semantic segmentation," *arXiv preprint arXiv:1811.12709*, 2018.
- [152] A. Kendall, V. Badrinarayanan, and R. Cipolla, "Bayesian SegNet: Model Uncertainty in Deep Convolutional Encoder-Decoder Architectures for Scene Understanding," Oct. 2016, arXiv:1511.02680 [cs].
- [153] P.-Y. Huang, W.-T. Hsu, C.-Y. Chiu, T.-F. Wu, and M. Sun, "Efficient uncertainty estimation for semantic segmentation in videos," in *ECCV*, 2018, pp. 520–535.

- [154] M. Kampffmeyer, A.-B. Salberg, and R. Jenssen, "Semantic segmentation of small objects and modeling of uncertainty in urban remote sensing images using deep convolutional neural networks," in *IEEE/CVF CVPR*, 2016, pp. 1–9.
- [155] C. Dechesne, P. Lassalle, and S. Lefèvre, "Bayesian u-net: Estimating uncertainty in semantic segmentation of earth observation images," *Remote Sensing*, vol. 13, no. 19, p. 3836, 2021.
- [156] D. Morrison, A. Milan, and E. Antonakos, "Uncertainty-aware instance segmentation using dropout sampling," in *Proceedings of the Robotic Vision Probabilistic Object Detection Challenge (CVPR 2019 Workshop)*, Long Beach, CA, USA, 2019, pp. 16–20.
- [157] C. Qi, J. Yin, Y. Niu, and J. Xu, "Neighborhood spatial aggregation mc dropout for efficient uncertainty-aware semantic segmentation in point clouds," *IEEE Transactions on Geoscience and Remote Sensing*, 2023.
- [158] Z. Eaton-Rosen, F. Bragman, S. Bisdas, S. Ourselin, and M. J. Cardoso, "Towards safe deep learning: accurately quantifying biomarker uncertainty in neural network predictions," in *MICCAI*. Springer, 2018, pp. 691–699.
- [159] A. Jungo, R. McKinley, R. Meier, U. Knecht, L. Vera, J. Pérez-Beteta, D. Molina-García, V. M. Pérez-García, R. Wiest, and M. Reyes, "Towards uncertainty-assisted brain tumor segmentation and survival prediction," in *BrainLes workshop, MICCAI*. Springer, 2018, pp. 474–485.
- [160] A. Jungo, R. Meier, E. Ermis, E. Herrmann, and M. Reyes, "Uncertainty-driven sanity check: application to postoperative brain tumor cavity segmentation," *arXiv preprint arXiv:1806.03106*, 2018.
- [161] A. G. Roy, S. Conjeti, N. Navab, and C. Wachinger, "Bayesian quicknat: Model uncertainty in deep whole-brain segmentation for structure-wise quality control," *NeuroImage*, vol. 195, pp. 11–22, 2018.
- [162] —, "Inherent brain segmentation quality control from fully convnet monte carlo sampling," in *MICCAI*. Springer, 2018, pp. 664–672.
- [163] A. Mehrtash, W. M. Wells, C. M. Tempny, P. Abolmaesumi, and T. Kapur, "Confidence Calibration and Predictive Uncertainty Estimation for Deep Medical Image Segmentation," *IEEE Trans. Med. Imag.*, vol. 39, no. 12, pp. 3868–3878, Dec. 2020.
- [164] T. Nair, D. Precup, D. L. Arnold, and T. Arbel, "Exploring uncertainty measures in deep networks for multiple sclerosis lesion detection and segmentation," *Medical image analysis*, vol. 59, p. 101557, 2020.
- [165] J. Sander, B. D. de Vos, J. M. Wolterink, and I. Išgum, "Towards increased trustworthiness of deep learning segmentation methods on cardiac mri," in *Medical imaging 2019: image Processing*, vol. 10949. SPIE, 2019, pp. 324–330.
- [166] S. K. Hasan and C. A. Linte, "Joint segmentation and uncertainty estimation of ventricular structures from cardiac mri using a bayesian condenseunet," in *2022 44th Annual International Conference of the IEEE Engineering in Medicine & Biology Society (EMBC)*. IEEE, 2022, pp. 5047–5050.
- [167] R. Camarasa, D. Bos, J. Hendrikse, P. Nederkoorn, M. E. Kooi, A. van der Lugt, and M. de Bruijne, "A quantitative comparison of epistemic uncertainty maps applied to multi-class segmentation," *arXiv preprint arXiv:2109.10702*, 2021.
- [168] S. Sedai, B. J. Antony, D. Mahapatra, and R. Garnavi, "Joint segmentation and uncertainty visualization of retinal layers in optical coherence tomography images using bayesian deep learning," *ArXiv*, vol. abs/1809.04282, 2018.
- [169] P. Seeböck, J. I. Orlando, T. Schlegl, S. M. Waldstein, H. Bogunović, S. Klimescha, G. Langs, and U. M. Schmidt-Erfurth, "Exploiting epistemic uncertainty of anatomy segmentation for anomaly detection in retinal oct," *IEEE Trans. Med. Imag.*, vol. 39, pp. 87–98, 2019.
- [170] T. DeVries and G. W. Taylor, "Leveraging uncertainty estimates for predicting segmentation quality," *arXiv preprint arXiv:1807.00502*, 2018.
- [171] S. Czolbe, K. Arnavaz, O. Krause, and A. Feragen, "Is segmentation uncertainty useful?" in *Information Processing in Medical Imaging: 27th International Conference, IPMI 2021, Virtual Event, June 28–June 30, 2021, Proceedings 27*. Springer, 2021, pp. 715–726.
- [172] K. Hoebel, K. Chang, J. Patel, P. Singh, and J. Kalpathy-Cramer, "Give me (un)certainty – An exploration of parameters that affect segmentation uncertainty," Nov. 2019, arXiv:1911.06357 [cs, eess].
- [173] I. Bhat, H. J. Kuijff, V. Cheplygina, and J. P. Pluim, "Using uncertainty estimation to reduce false positives in liver lesion detection," in *2021 IEEE 18th International Symposium on Biomedical Imaging (ISBI)*. IEEE, 2021, pp. 663–667.
- [174] M. Antico, F. Sasazawa, Y. Takeda, A. T. Jaiprakash, M.-L. Wille, A. K. Pandey, R. Crawford, G. Carneiro, and D. Fontanarosa, "Bayesian cnn for segmentation uncertainty inference on 4d ultrasound images of the femoral cartilage for guidance in robotic knee arthroscopy," *IEEE access*, vol. 8, pp. 223 961–223 975, 2020.
- [175] J. L. Rumberger, L. Mais, and D. Kaimueller, "Probabilistic deep learning for instance segmentation," in *ECCV*. Springer, 2020, pp. 445–457.
- [176] E. Hann, I. A. Popescu, Q. Zhang, R. A. Gonzales, A. Barutcu, S. Neubauer, V. M. Ferreira, and S. K. Piechnik, "Deep neural network ensemble for on-the-fly quality control-driven segmentation of cardiac MRI T1 mapping," *Medical Image Analysis*, vol. 71, p. 102029, Jul. 2021.
- [177] G. Carannante, D. Dera, N. C. Bouaynaya, H. M. Fathallah-Shaykh, and G. Rasool, "Super-net: Trustworthy medical image segmentation with uncertainty propagation in encoder-decoder networks," 2021.
- [178] S. K. Hasan and C. A. Linte, "Calibration of cine mri segmentation probability for uncertainty estimation using a multi-task cross-task learning architecture," in *Medical Imaging 2022: Image-Guided Procedures, Robotic Interventions, and Modeling*, vol. 12034. SPIE, 2022, pp. 174–179.
- [179] T. LaBonte, C. Martinez, and S. A. Roberts, "We know where we don't know: 3d bayesian cnns for credible geometric uncertainty," *arXiv preprint arXiv:1910.10793*, 2019.
- [180] J. Linmans, J. van der Laak, and G. Litjens, "Efficient out-of-distribution detection in digital pathology using multi-head convolutional neural networks," in *MIDL*, 2020, pp. 465–478.
- [181] S. Pavlitskaya, C. Hubschneider, M. Weber, R. Moritz, F. Huger, P. Schlicht, and J. M. Zollner, "Using Mixture of Expert Models to Gain Insights into Semantic Segmentation," in *2020 IEEE/CVF Conference on Computer Vision and Pattern Recognition Workshops (CVPRW)*. Seattle, WA, USA: IEEE, Jun. 2020, pp. 1399–1406.
- [182] O. Ozdemir, B. Woodward, and A. A. Berlin, "Propagating uncertainty in multi-stage bayesian convolutional neural networks with application to pulmonary nodule detection," *arXiv preprint arXiv:1712.00497*, 2017.
- [183] C. Bian, C. Yuan, J. Wang, M. Li, X. Yang, S. Yu, K. Ma, J. Yuan, and Y. Zheng, "Uncertainty-aware domain alignment for anatomical structure segmentation," *Medical Image Analysis*, vol. 64, p. 101732, Aug. 2020.
- [184] S. Iwamoto, B. Raytchev, T. Tamaki, and K. Kaneda, "Improving the reliability of semantic segmentation of medical images by uncertainty modeling with bayesian deep networks and curriculum learning," in *UNSURE workshop, MICCAI*. Springer, 2021, pp. 34–43.
- [185] Y. Li, X. Chen, L. Quan, and N. Zhang, "Uncertainty-guided robust training for medical image segmentation," in *2021 IEEE 18th International Symposium on Biomedical Imaging (ISBI)*. IEEE, 2021, pp. 1471–1475.
- [186] A. Valada, A. Dhall, and W. Burgard, "Convolved mixture of deep experts for robust semantic segmentation," in *IEEE/RSJ IROS workshop, state estimation and terrain perception for all terrain mobile robots*, vol. 2, 2016, p. 1.
- [187] A. Valada, J. Vertens, A. Dhall, and W. Burgard, "Adapnet: Adaptive semantic segmentation in adverse environmental conditions," in *2017 IEEE International Conference on Robotics and Automation (ICRA)*. IEEE, 2017, pp. 4644–4651.
- [188] K. Kamnitsas, W. Bai, E. Ferrante, S. McDonagh, M. Sinclair, N. Pawlowski, M. Rajchl, M. Lee, B. Kainz, D. Rueckert *et al.*, "Ensembles of multiple models and architectures for robust brain tumour segmentation," in *BrainLes workshop, MICCAI*. Springer, 2018, pp. 450–462.
- [189] K. Hoebel, V. Andrearczyk, A. L. Beers, J. B. Patel, K. Chang, A. Depeursinge, H. Mueller, and J. Kalpathy-Cramer, "An exploration of uncertainty information for segmentation quality assessment," in *Medical Imaging 2020: Image Processing*, B. A. Landman and I. Išgum, Eds. Houston, United States: SPIE, Mar. 2020, p. 55.
- [190] K. Wickström, M. Kampffmeyer, and R. Jenssen, "Uncertainty and interpretability in convolutional neural networks for semantic segmentation of colorectal polyps," *Medical image analysis*, vol. 60, p. 101619, 2020.
- [191] B. Settles, "Active learning literature survey," 2009.
- [192] P. Ren, Y. Xiao, X. Chang, P.-Y. Huang, Z. Li, B. B. Gupta, X. Chen, and X. Wang, "A survey of deep active learning," *ACM computing surveys (CSUR)*, vol. 54, no. 9, pp. 1–40, 2021.
- [193] N. Housley, F. Huszár, Z. Ghahramani, and M. Lengyel, "Bayesian active learning for classification and preference learning," *arXiv preprint arXiv:1112.5745*, 2011.
- [194] J.-M. Burmeister, M. F. Rosas, J. Hagemann, J. Kordt, J. Blum, S. Shabo, B. Bergner, and C. Lippert, "Less is more: A comparison of

- active learning strategies for 3d medical image segmentation,” *arXiv preprint arXiv:2207.00845*, 2022.
- [195] Z. Zhao, Z. Zeng, K. Xu, C. Chen, and C. Guan, “Dsal: Deeply supervised active learning from strong and weak labelers for biomedical image segmentation,” *IEEE journal of biomedical and health informatics*, vol. 25, no. 10, pp. 3744–3751, 2021.
- [196] L. Yang, Y. Zhang, J. Chen, S. Zhang, and D. Z. Chen, “Suggestive annotation: A deep active learning framework for biomedical image segmentation,” in *Medical Image Computing and Computer Assisted Intervention- MICCAI 2017: 20th International Conference, Quebec City, QC, Canada, September 11-13, 2017, Proceedings, Part III 20*. Springer, 2017, pp. 399–407.
- [197] M. Shen, J. Y. Zhang, L. Chen, W. Yan, N. Jani, B. Sutton, and O. Koyejo, “Labeling cost sensitive batch active learning for brain tumor segmentation,” in *2021 IEEE 18th International Symposium on Biomedical Imaging (ISBI)*. IEEE, 2021, pp. 1269–1273.
- [198] M. Gorriz, A. Carlier, E. Faure, and X. Giro-i Nieto, “Cost-effective active learning for melanoma segmentation,” *arXiv preprint arXiv:1711.09168*, 2017.
- [199] N. Khalili, J. Spronck, F. Ciompi, J. van der Laak, and G. Litjens, “Uncertainty-guided annotation enhances segmentation with the human-in-the-loop,” *arXiv preprint arXiv:2404.07208*, 2024.
- [200] S. Ma, H. Wu, A. Lawlor, and R. Dong, “Breaking the barrier: Selective uncertainty-based active learning for medical image segmentation,” *arXiv preprint arXiv:2401.16298*, 2024.
- [201] B. Li and T. S. Alstrøm, “On uncertainty estimation in active learning for image segmentation,” *arXiv preprint arXiv:2007.06364*, 2020.
- [202] Y. Siddiqui, J. Valentin, and M. Nießner, “Viewal: Active learning with viewpoint entropy for semantic segmentation,” in *IEEE/CVF CVPR*, 2020, pp. 9433–9443.
- [203] C. García Rodríguez, J. Vitrià, and O. Mora, “Uncertainty-based human-in-the-loop deep learning for land cover segmentation,” *Remote Sensing*, vol. 12, no. 22, p. 3836, 2020.
- [204] T. Kasarla, G. Nagendar, G. M. Hegde, V. Balasubramanian, and C. Jawahar, “Region-based active learning for efficient labeling in semantic segmentation,” in *2019 IEEE winter conference on applications of computer vision (WACV)*. IEEE, 2019, pp. 1109–1117.
- [205] T.-H. Wu, Y.-C. Liu, Y.-K. Huang, H.-Y. Lee, H.-T. Su, P.-C. Huang, and W. H. Hsu, “Redal: Region-based and diversity-aware active learning for point cloud semantic segmentation,” in *IEEE/CVF ICCV*, 2021, pp. 15510–15519.
- [206] Z. Wu, L. Wang, W. Wang, Q. Xia, C. Chen, A. Hao, and S. Li, “Pixel is all you need: adversarial trajectory-ensemble active learning for salient object detection,” in *Proceedings of the AAAI Conference on Artificial Intelligence*, vol. 37, no. 3, 2023, pp. 2883–2891.
- [207] C. Cremer, “Inference suboptimality in variational autoencoders,” *arXiv preprint arXiv:1801.03558*, 2018.
- [208] H. Zheng, W. Nie, A. Vahdat, K. Aizzadenesheli, and A. Anandkumar, “Fast sampling of diffusion models via operator learning,” in *International conference on machine learning*. PMLR, 2023, pp. 42390–42402.
- [209] C. Meng, R. Rombach, R. Gao, D. Kingma, S. Ermon, J. Ho, and T. Salimans, “On distillation of guided diffusion models,” in *Proceedings of the IEEE/CVF Conference on Computer Vision and Pattern Recognition*, 2023, pp. 14297–14306.
- [210] A. Q. Nichol and P. Dhariwal, “Improved denoising diffusion probabilistic models,” in *ICML*. PMLR, 2021, pp. 8162–8171.
- [211] M. Arjovsky and L. Bottou, “Towards principled methods for training generative adversarial networks,” *arXiv preprint arXiv:1701.04862*, 2017.
- [212] L. L. Folgoc, V. Baltatzis, S. Desai, A. Devaraj, S. Ellis, O. E. M. Manzanera, A. Nair, H. Qiu, J. Schnabel, and B. Glocker, “Is mc dropout bayesian?” *arXiv preprint arXiv:2110.04286*, 2021.
- [213] I. Osband, “Risk versus uncertainty in deep learning: Bayes, bootstrap and the dangers of dropout,” in *NeurIPS workshop on bayesian deep learning*, vol. 192. MIT Press, 2016.
- [214] X. Guo, Y. Yang, C. Ye, S. Lu, Y. Xiang, and T. Ma, “Accelerating Diffusion Models via Pre-segmentation Diffusion Sampling for Medical Image Segmentation,” Oct. 2022, arXiv:2210.17408 [cs, eess].
- [215] K. Zepf, E. Petersen, J. Frellsen, and A. Feragen, “That label’s got style: Handling label style bias for uncertain image segmentation,” *arXiv preprint arXiv:2303.15850*, 2023.
- [216] K. Zepf, J. Frellsen, and A. Feragen, “Navigating uncertainty in medical image segmentation,” in *2024 IEEE International Symposium on Biomedical Imaging (ISBI)*. IEEE, 2024, pp. 1–5.
- [217] S. Ma, P. Mathur, Z. Ju, A. Lawlor, and R. Dong, “Model-data-driven adversarial active learning for brain tumor segmentation,” *Computers in Biology and Medicine*, vol. 176, p. 108585, 2024.
- [218] G. Li, C. Li, C. Zeng, P. Gao, and G. Xie, “Region Focus Network for Joint Optic Disc and Cup Segmentation,” *Proceedings of the AAAI Conference on Artificial Intelligence*, vol. 34, no. 01, pp. 751–758, Apr. 2020.
- [219] X. O. He, “Mixture of a million experts,” *arXiv preprint arXiv:2407.04153*, 2024.
- [220] J. Mukhoti, A. Kirsch, J. van Amersfoort, P. H. Torr, and Y. Gal, “Deep deterministic uncertainty: A new simple baseline,” in *IEEE/CVF CVPR*, 2023, pp. 24384–24394.
- [221] J. Liu, Z. Lin, S. Padhy, D. Tran, T. Bedrax Weiss, and B. Lakshminarayanan, “Simple and principled uncertainty estimation with deterministic deep learning via distance awareness,” *Advances in neural information processing systems*, vol. 33, pp. 7498–7512, 2020.
- [222] J. Van Amersfoort, L. Smith, Y. W. Teh, and Y. Gal, “Uncertainty estimation using a single deep deterministic neural network,” in *International conference on machine learning*. PMLR, 2020, pp. 9690–9700.
- [223] A. Dempster, “Upper and lower probabilities induced by multivalued mapping, a. of mathematical statistics, ed.” *AMS-38*, vol. 10, 1967.
- [224] M. Sensoy, L. Kaplan, and M. Kandemir, “Evidential deep learning to quantify classification uncertainty,” *NeurIPS*, vol. 31, 2018.
- [225] S. Ancha, P. R. Osteen, and N. Roy, “Deep evidential uncertainty estimation for semantic segmentation under out-of-distribution obstacles,” in *Proc. IEEE Int. Conf. Robot. Autom.*, 2024.
- [226] A. Vaswani, N. Shazeer, N. Parmar, J. Uszkoreit, L. Jones, A. N. Gomez, Ł. Kaiser, and I. Polosukhin, “Attention is all you need,” *NeurIPS*, vol. 30, 2017.
- [227] E. Xie, W. Wang, Z. Yu, A. Anandkumar, J. M. Alvarez, and P. Luo, “Segformer: Simple and efficient design for semantic segmentation with transformers,” *NeurIPS*, vol. 34, pp. 12077–12090, 2021.
- [228] Q. Zhang and Y.-B. Yang, “Rest: An efficient transformer for visual recognition,” *NeurIPS*, vol. 34, pp. 15475–15485, 2021.
- [229] C. Hümmer, M. Schwonberg, L. Zhong, H. Cao, A. Knoll, and H. Gottschalk, “Vltseg: Simple transfer of clip-based vision-language representations for domain generalized semantic segmentation,” *arXiv preprint arXiv:2312.02021*, 2023.
- [230] M. Caron, H. Touvron, I. Misra, H. Jégou, J. Mairal, P. Bojanowski, and A. Joulin, “Emerging properties in self-supervised vision transformers,” in *Proceedings of the IEEE/CVF international conference on computer vision*, 2021, pp. 9650–9660.
- [231] Z. Liu, H. Mao, C.-Y. Wu, C. Feichtenhofer, T. Darrell, and S. Xie, “A convnet for the 2020s,” in *IEEE/CVF CVPR*, 2022, pp. 11976–11986.
- [232] A. N. Angelopoulos and S. Bates, “A gentle introduction to conformal prediction and distribution-free uncertainty quantification,” *arXiv preprint arXiv:2107.07511*, 2021.
- [233] H. Wieslander, P. J. Harrison, G. Skogberg, S. Jackson, M. Fridén, J. Karlsson, O. Spjuth, and C. Wählby, “Deep learning with conformal prediction for hierarchical analysis of large-scale whole-slide tissue images,” *IEEE journal of biomedical and health informatics*, vol. 25, no. 2, pp. 371–380, 2020.
- [234] J. Brunkreef, E. Marcus, R. Sheombarsing, J.-J. Sonke, and J. Teuwen, “Kandinsky conformal prediction: Efficient calibration of image segmentation algorithms,” in *Proceedings of the IEEE/CVF Conference on Computer Vision and Pattern Recognition*, 2024, pp. 4135–4143.
- [235] L. Mossina, J. Dalmau, and L. Andéol, “Conformal semantic image segmentation: Post-hoc quantification of predictive uncertainty,” in *Proceedings of the IEEE/CVF Conference on Computer Vision and Pattern Recognition*, 2024, pp. 3574–3584.
- [236] A. M. Wundram, P. Fischer, M. Mühlebach, L. M. Koch, and C. F. Baumgartner, “Conformal performance range prediction for segmentation output quality control,” in *International Workshop on Uncertainty for Safe Utilization of Machine Learning in Medical Imaging*. Springer, 2024, pp. 81–91.